

# The antiretroviral 2',3'-dideoxycytidine causes mitochondrial dysfunction in proliferating and differentiated HepaRG human cell cultures

Received for publication, June 23, 2020, and in revised form, December 15, 2020. Published, Paper in Press, December 17, 2020,

<https://doi.org/10.1074/jbc.RA120.014885>

Carolyn K.J. Young<sup>1</sup>, Joel H. Wheeler, Md. Mostafijur Rahman<sup>1</sup>, and Matthew J. Young<sup>1\*</sup>

From the Department of Biochemistry and Molecular Biology, Southern Illinois University School of Medicine, Carbondale, Illinois, USA

Edited by Craig Cameron

Nucleoside reverse transcriptase inhibitors (NRTIs) were the first drugs used to treat human immunodeficiency virus infection, and their use can cause mitochondrial toxicity, including mitochondrial DNA (mtDNA) depletion in several cases. The first-generation NRTIs, including 2',3'-dideoxycytidine (ddC), were originally and are still pursued as anti-cancer agents. NRTI-sensitive DNA polymerases localizing to mitochondria allow for the opportunity to poison proliferating cancer cell mtDNA replication as certain cancers rely heavily on mitochondrial functions. However, mtDNA replication is independent of the cell cycle creating a significant concern that toxicants such as ddC impair mtDNA maintenance in both proliferating and nonproliferating cells. To examine this possibility, we tested the utility of the HepaRG cell line to study ddC-induced toxicity in isogenic proliferating (undifferentiated) and nonproliferating (differentiated) cells. Following ddC exposures, we measured cell viability, mtDNA copy number, and mitochondrial bioenergetics utilizing trypan blue, Southern blotting, and extracellular flux analysis, respectively. After 13 days of 1  $\mu$ M ddC exposure, proliferating and differentiated HepaRG harbored mtDNA levels of 0.9% and 17.9% compared with control cells, respectively. Cells exposed to 12  $\mu$ M ddC contained even less mtDNA. By day 13, differentiated cell viability was maintained but declined for proliferating cells. Proliferating HepaRG bioenergetic parameters were severely impaired by day 8, with 1 and 12  $\mu$ M ddC, whereas differentiated cells displayed defects of spare and maximal respiratory capacities (day 8) and proton-leak linked respiration (day 14) with 12  $\mu$ M ddC. These results indicate HepaRG is a useful model to study proliferating and differentiated cell mitochondrial toxicant exposures.

In human immunodeficiency virus (HIV)-infected patients, nucleoside reverse transcriptase inhibitors (NRTIs) are used to inhibit the reverse transcription of the single-stranded HIV RNA genome into double-stranded DNA. Reverse transcription is carried out by the HIV reverse transcriptase. NRTIs are typically used in combination with other anti-HIV drugs, such

as nonnucleotide reverse transcriptase inhibitors, protease inhibitors, integrase strand transfer inhibitors, fusion inhibitors, and chemokine receptor (CCR5) antagonists in scheduled regimens called antiretroviral therapy (1). One potent US Food and Drug Administration-approved NRTI is 2',3'-dideoxycytidine (ddC), also known as zalcitabine. ddC has been documented to cause unexpected sensorineural deafness, hypertrophic cardiomyopathy, peripheral neuropathy, mitochondrial alterations, and reduced mitochondrial DNA (mtDNA) copy number (2–4). Nucleotide reverse transcriptase inhibitors (NtRTIs) are generated *in vivo* via phosphorylation of NRTIs by intracellular kinases (5) or occur in a monophosphate bioisostere form (nucleoside phosphonate) such as in the case of tenofovir (PMPA). Nucleoside kinases such as DCK, CMPK1, and nucleoside diphosphate kinases (NME) act on NRTIs, such as ddC, and perform the first, second, and third phosphorylation steps, respectively, generating the metabolically active NtRTI ddCTP in the cytoplasm (6). Once imported into mitochondria, NtRTIs can compete with native nucleotides for DNA polymerase active sites to inhibit mtDNA replication through chain termination. Unlike natural deoxyribonucleotide triphosphate substrates, most NtRTIs lack the 3' hydroxyl group (3'-OH) and therefore cannot be extended by a polymerase once incorporated into DNA. As a derivative of deoxycytidine, ddC possesses a 3' hydrogen in place of the deoxycytidine 3'-OH; thus, if ddCMP is not removed from the nascent mtDNA strand *in vivo*, replication will stall. Several DNA polymerases that localize to the mitochondrion, including the replicative mtDNA polymerase gamma (Poly), are sensitive to inhibition by ddCTP. Anti-HIV NtRTIs including ddCTP, AZT-TP (3'-azido-2',3'-dideoxythymidine triphosphate), 3TC-TP (2',3'-dideoxy-3'-thiacytidine triphosphate), D4T-TP (2',3'-didehydro-2',3'-dideoxythymidine triphosphate), and carbovir triphosphate (CBV-TP) have been demonstrated to inhibit the nucleotide insertion activity of an exonuclease deficient version of the Poly p140 catalytic subunit *in vitro*. Furthermore, when a WT version of p140 was separately incubated with DNA substrates containing different 3'-terminal analogs (ddCMP, AZT-MP, 3TC-MP, D4T-MP, or CBV-MP) their exonucleolytic removals were compromised in comparison with control substrates (7). Similarly, the Poly

This article contains [supporting information](#).

\* For correspondence: Matthew J. Young, [matthew.young@siu.edu](mailto:matthew.young@siu.edu).

## Utilizing HepaRG to understand ddC mitochondrial toxicity

holoenzyme was demonstrated to remove 3'-end ddCMP, AZT-MP, 3TC-MP, D4T-MP, or CBV-MP from separate primer-template complexes slower than from a control substrate complex harboring a correctly paired dCMP (8, 9). In contrast, the nuclear DNA (nDNA) polymerases alpha ( $\alpha$ ), delta ( $\delta$ ), and epsilon ( $\epsilon$ ) harbor strong nucleotide selection mechanisms and are less likely to incorporate NRTIs (3, 10).

Support for intracellular NRTI/ddC mitochondria toxicity mediated by disruption of mtDNA replication comes from observations that primary and immortalized proliferating cell lines undergo mtDNA depletion upon exposure to various NRTIs (3). In the case of ddC, mtDNA depletion has been observed in primary cell lines such as skeletal muscle cells (1° SkMCs), renal proximal tubule epithelial cells (1° RPTECs), peripheral blood lymphocytes (1° PBLs), as well as cell lines derived from prostate metastatic carcinoma (PC-3), leukemia (MOLT-4 and CEM), hepatocellular carcinoma (HepG2), cervical cancer (HeLa), and other immortalized cell lines (3, 11–16). Examples of other NRTIs that have been demonstrated to cause reduced mtDNA copy number in cell lines include ddI (2',3'-dideoxyinosine in CEM, HepG2, 1° SkMCs, 1° RPTECs, and 1° PBLs), 2',3'-dideoxy-2',3'-dideoxythymidine (in CEM, MOLT-4, HepG2, 1° SkMCs, 1° RPTECs, 1° PBLs, and immortalized human mesenchymal/stromal cell lines, hMSCs), and AZT (in HepG2 and hMSC) (3, 11, 12, 14, 15, 17). The documented NRTI-associated mitochondrial toxicities and resulting manifestations observed in patients have prompted investigations into drug and environmental factors that function as mitochondrial toxicants. Details regarding mitochondrial toxicants have been thoroughly reviewed (3, 18–20).

Off-target effects of drugs and environmental toxicants causing mitochondrial dysfunction are important factors to consider in toxicity studies, and human cell lines have served as useful models for these experiments (3, 21, 22). The use of *in vitro* human cell culture models in toxicity testing is becoming increasingly attractive owing to the small quantities of compounds needed for testing, shortened experimental timelines, increased throughput to evaluate toxicants, and reduced number and suffering of animals (23, 24). Primary human hepatocytes isolated from liver and liver-derived immortalized cell lines are widely used as models for toxicological studies as the liver is the primary source of drug metabolism and biotransformation (23). The HepaRG cell line was originally derived from a liver tumor obtained from a patient with hepatitis C infection and hepatocarcinoma (25). Genetically, HepaRG has been demonstrated to have a highly stable pseudo-diploid karyotype (25, 26). HepaRG is a proliferating human cell line that can be differentiated into nonproliferating hepatocyte-like and biliary-like cells (27–30). Differentiated HepaRG cultures have been demonstrated to suffer toxicity from compounds metabolized *via* cytochrome P450s (28). Previously, we utilized HepaRG to gain insight into both undifferentiated proliferating and quiescent differentiated cell metabolism when isogenic cells were exposed to acetaminophen (APAP) and the biguanide metformin (31). We showed that metformin offers protection against loss of APAP-induced cellular viability and prevents APAP-induced decreases

in bioenergetics in differentiated but not proliferating-derived HepaRG. It could be distinguished that treatment with metformin alone reduced the mitochondrial bioenergetic parameters ATP-linked respiration, maximal respiratory capacity, and basal respiration in proliferating-derived cells. In addition, we recently performed mtDNA next-generation sequencing and reported the HepaRG mtDNA sequence including its haplogroup branch H15a1 polymorphisms and levels of heteroplasmy (32). In comparison with the revised Cambridge Reference Sequence, HepaRG mtDNA contains 14 nucleotide variations including two heteroplasmic variants, the noncoding control region variant 315insC at 42%, and the novel G13633A *ND5* gene substitution at 33% heteroplasmy.

NRTI-sensitive DNA polymerases localizing to mitochondria afford a unique opportunity to poison proliferating cancer cell mitochondria as certain cancers have an increased reliance on oxidative phosphorylation (OXPHOS), and nDNA polymerases are less sensitive to NRTI inhibition (6, 14). Of interest, nucleoside analogs were originally studied as antimetabolites in the 1950s and the first-generation NRTIs such as ddC, ddI, and AZT were originally pursued as anticancer agents (33–35). Also, the antibacterial activity of AZT has been reported (36). In 1985 and 1986, these three NRTIs were demonstrated to be anti-HIV agents (37). Different cancer types undergo different bioenergetic alterations with some being more glycolytic and others being more oxidative (38). When treated with ddC, proliferating acute myeloid leukemia cells preferentially activated the analog and blocked mtDNA replication and OXPHOS in comparison with hematopoietic cells (6). Also, ddC was proposed to be used for treating tumors with high levels of expression of DNA polymerase beta ( $\text{Pol}\beta$ ) (39). Furthermore, the combined use of AZT and ddI was shown to reduce tumor growth of human colorectal carcinoma HCT-116 cells in mice (40). As mammalian mtDNA replication takes place independently from the cell cycle (41–45) mtDNA maintenance disrupting drugs, such as ddC, will likely impair mitochondrial functions in both proliferating and nonproliferating cells. Furthermore, studying the effect of ddC on different cell types is necessary, as the bioenergetic consequence of ddC on quiescent differentiated cells has not been thoroughly investigated. Evaluation of the off-target effects of drugs on mitochondrial function using human cell lines is an important consideration for determining mitochondrial toxicity because the complex mitochondrial network harbors multiple copies of OXPHOS complexes and mtDNA that may cause a slow response to these agents. It must also be noted that HIV-infected patients have undergone chronic months-long treatments with ddC (2). To gain information about the mechanism of ddC mitochondrial toxicity, here we examine the effects of ddC exposure on proliferating and nonproliferating/differentiated HepaRG cell viability, mtDNA maintenance, and mitochondrial bioenergetics.

## Results

### *Differentiated HepaRG cells have higher levels of mtDNA than proliferating cells*

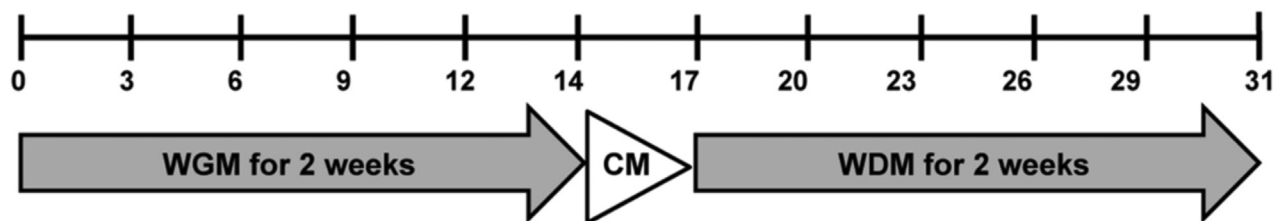
As mammalian mtDNA replication is independent of the cell cycle we wanted to determine mtDNA levels in both

## Utilizing HepaRG to understand ddC mitochondrial toxicity

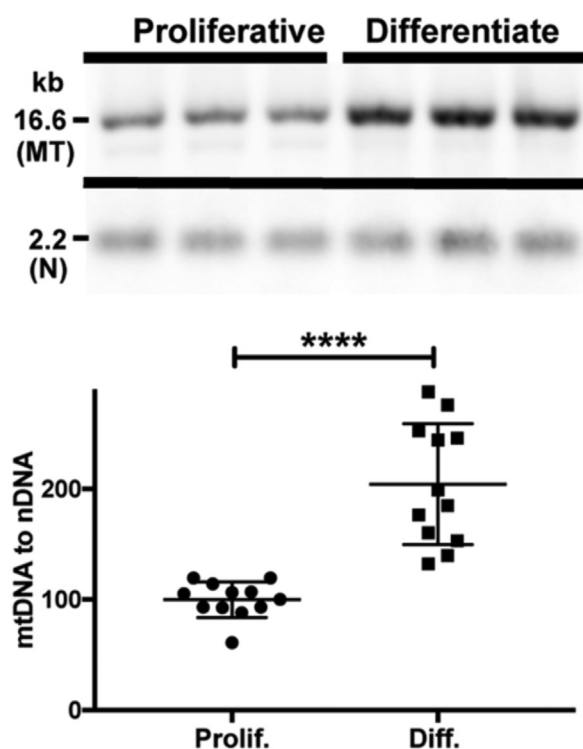
proliferating and differentiated HepaRG cell phases (41–45). DNA samples from both cell types were compared using Southern blotting and dual digoxigenin (DIG)-labeled probe hybridization to estimate mtDNA content. Proliferating HepaRG whole-cell extracted (WCE) DNA samples were prepared

from cells obtained at 7 days post-seeding at  $2 \times 10^4$  cells/cm<sup>2</sup>, and differentiated HepaRG DNA samples were prepared from cells harvested at 7 days post-differentiation, Figure 1A. The levels of mtDNA in each lane of the blot were detected with the mtDNA-specific probe and were normalized to nDNA

### A HepaRG differentiation timeline (31 days)



### B



### C

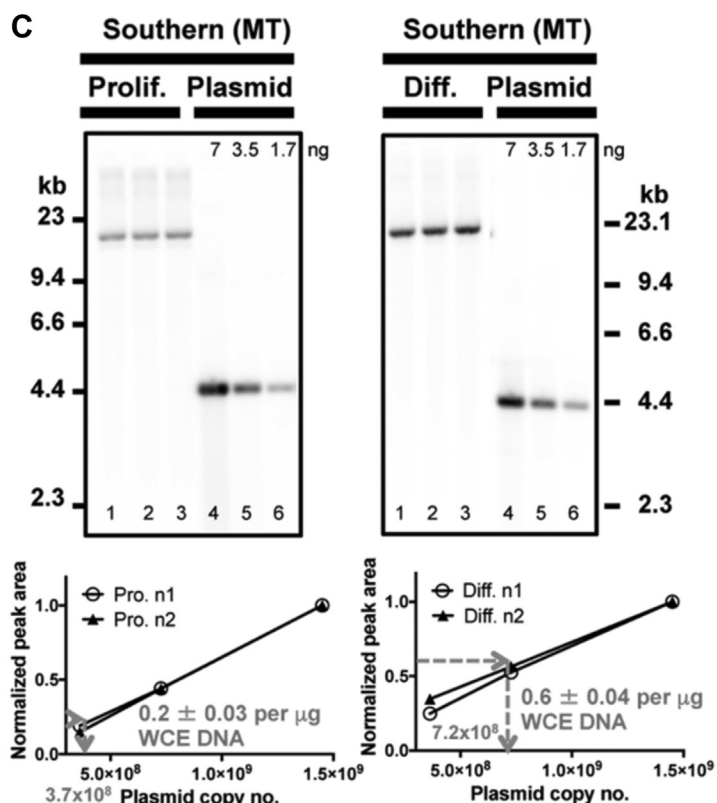


**Figure 1. HepaRG differentiation timeline and mitochondrial DNA (mtDNA) content.** A, timeline of HepaRG differentiation. CM, Combination Medium; WDM, Working Differentiation Medium; WGM, Working Growth Medium (see [Experimental procedures](#)). B, a representative Southern blot of relative proliferating and differentiated HepaRG mtDNA content. Triplicate 1 µg reactions of whole-cell extracted (WCE) DNA were digested with BamHI, then loaded and electrophoresed on an agarose gel before blotting. The Southern blot was probed simultaneously with mtDNA (MT) and nDNA (N) probes. Proliferating HepaRG WCE DNA samples were prepared from cells obtained 7 days post-seeding at  $2 \times 10^4$  cells/cm<sup>2</sup>. Differentiated HepaRG DNA samples were prepared from cells obtained 7 days post-differentiation. BamHI-digested human genomic DNA samples generate a 16.6-kb mtDNA genome-length band and a 2.2-kb nDNA band as described (79). Using the relative comparison of the MT to the N probe, differentiated HepaRG cells contain ~2-fold more mtDNA than proliferating cells. Data are presented as mean  $\pm$  standard deviation (SD);  $n = 12$  from  $n \geq 3$  whole-cell DNA extract preparations derived from independent passages. Four Southern blots containing triplicate sample replicates were used for the analysis. For each lane of the dual-probed blots, the mtDNA peak 'Percent' value was normalized to the 185 nDNA peak 'Percent' value. A peak percent value is defined as the area of a peak measured as a percent of the total size of all measured peak areas on a blot. The mean normalized band intensity values of the proliferating HepaRG samples were set to 100% (\*\*\*\* $p < 0.0001$ ). C, quantitation of mtDNA molecules per cell. Representative blots are shown for each of proliferating (Prolif.) and differentiated (Diff.) HepaRG. Triplicate 1 µg reactions of WCE DNA were digested with BamHI then loaded and electrophoresed on an agarose gel. In parallel, 7.0, 3.5, and 1.7 ng of HindIII linearized pCR2.1-TOPO-mtDNA plasmid (4.4-kb) were loaded. The blots were detected with the MT probe. Three-point standard curves based on the pCR2.1-TOPO-mtDNA peak area percent values were used to estimate the mtDNA copy number and the 7-ng plasmid bands were set to 1. Two curves from two blots are plotted below the representative blots. The average mtDNA peak area percent values for 1 µg proliferating or differentiated HepaRG whole-cell DNA extracts are shown in gray with errors reported as SD ( $n = 6$ ; triplicate measurements from two independent experiments using different passages; P10 and P14, differentiated; P8 and P9, proliferating HepaRG). On average, 1 µg of proliferating HepaRG WCE DNA was prepared from  $1.4 \times 10^5 \pm 4.4 \times 10^4$  cells and 1 µg of differentiated WCE DNA was prepared from  $9.8 \times 10^4 \pm 1.7 \times 10^4$  cells ( $n = 6$  for each; triplicate cell counts from two independent experiments using different passages). The calculated copies of mtDNA are  $3.7 \times 10^8$  mtDNA/µg or 2600 mtDNA genomes per proliferating cell and  $7.2 \times 10^8$ /µg or 7400 mtDNA genomes per differentiated cell.

## Utilizing HepaRG to understand ddC mitochondrial toxicity

levels detected with the 18S probe in the same lane, [Figure 1B](#). Using this relative comparison method, differentiated HepaRG contains ~2-fold more mtDNA compared with proliferating cells. Since differentiated cells are no longer undergoing cell division these cells likely maintain a higher level of mtDNA copy number that is necessary for mitochondrial bioenergetic functions.

Next, we determined the number of mtDNA molecules in WCE DNA samples using Southern blotting and the mtDNA DIG-labeled probe. Three-point standard curves of known quantities of linearized pCR2.1-TOPO-mtDNA plasmid harboring the mtDNA template sequence used to generate the mtDNA probe were loaded onto gels in parallel with WCE DNA samples. The number of mtDNA molecules in proliferating and differentiated HepaRG WCE DNA samples was calculated utilizing linear regression analysis of plasmid band intensities (peak area percent values), [Figure 1C](#). In good agreement with the dual probe (relative comparison) method, we calculated there are at least 2600 and 7400 mtDNA genomes per proliferating and differentiated HepaRG cell, respectively (2.9-fold more mtDNA per differentiated cell). By comparison, using a dot blot hybridization technique, human 143B cybrid cell lines were reported to harbor an average of 13,000 wild-type mtDNA genomes per cell ([46](#)).

### Proliferating HepaRG cell growth is inhibited by exposure to ddC

Cell survival was determined by counting the number of viable cells utilizing the trypan blue exclusion method. The doubling time of proliferating HepaRG under standard tissue culture conditions is  $44 \pm 4$  h; the error reported is the standard deviation (SD), [Figure 2A](#). Assuming that during ddC treatment the proliferating cells continue to divide, mtDNA replication is blocked, and that following a cell division parental cell mtDNA (2600 mtDNA/cell) is equally distributed among daughter cells, then after 15 days of treatment, we would expect mtDNAs per cell to be <1% of initial levels. Here we examined a range of concentrations from 0 to 128  $\mu\text{M}$  that included 0.5 and 1  $\mu\text{M}$  ddC, as peak plasma concentrations of 0.5 and 1  $\mu\text{M}$  ddC have been reported in patients ([47](#), [48](#)), [Figure 2](#), B–C. Of interest, ddC likely accumulates at different concentrations within different organs and tissues as indicated by an experiment using rats where differences in unbound ddC distribution have been measured. Rat muscle contained ~8-fold higher concentrations of ddC compared with the brain, 238 and 31  $\mu\text{M}$ , respectively ([49](#)). We determined the half-maximal inhibitory concentration ( $\text{IC}_{50}$ ) value or concentration of ddC, which reduces the number of viable treated cells by 50% relative to untreated control cells. Following 15 days of ddC treatment, we observed the recognizable symmetrical sigmoidal shape of  $\log(\text{toxicant})$  versus percent cell survival for proliferating HepaRG, [Figure 2B](#). When examining the number of live cells remaining post-treatment and normalizing to untreated cells, proliferating HepaRG growth and survival was inhibited by 50% at  $0.2 \pm 0.05$   $\mu\text{M}$  ddC. This value is similar to the  $\text{IC}_{50}$

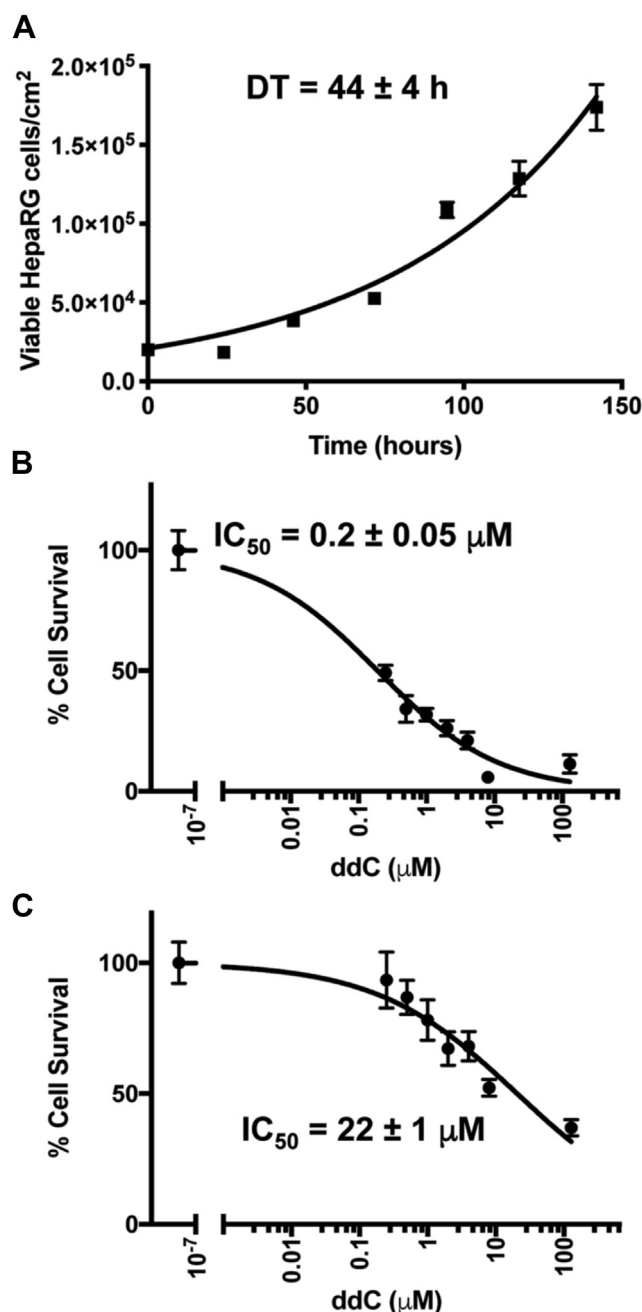


**Figure 2. HepaRG growth rate and survival following 2',3'-dideoxycytidine (ddC) treatment.** A, proliferating HepaRG growth rate was determined by growing cells in Working Growth Medium (WGM) at 5% CO<sub>2</sub>, 37 °C. Cells were seeded at  $2 \times 10^4$  cells/cm<sup>2</sup>. The mean doubling time (DT) based on three independent experiments utilizing HepaRG at passages P8, P9, and P16 is reported in hours (h) with error as SD. Mean viable cell count values (n = 4) and SDs for a representative experiment (P8) are shown in the graph. DT values were calculated using the least-squares fit of the exponential growth equation in Graph Pad Prism. B, a representative proliferating HepaRG survival curve is shown following exposure to ddC. The mean  $\text{IC}_{50}$  value based on two independent experiments utilizing HepaRG at passages P15 and P16 is reported in micromolar ( $\mu\text{M}$ ) with error as SD. Cells were seeded at  $2 \times 10^4$  cells/cm<sup>2</sup> in WGM the day before the addition of WGM treatment media. C, a representative differentiated HepaRG survival curve is shown following exposure to Working Differentiation Medium ddC treatment media. The mean  $\text{IC}_{50}$  value based on two independent experiments utilizing differentiated cells at passages P8 and P10 is reported in micromolar with error as SD. In B, proliferating and C, differentiated experiments, cells were exposed to 128, 8, 4, 2, 1, 0.5, 0.25, and 0  $\mu\text{M}$  ddC for 15 days, and mean survival values (n ≥ 3) and SDs are reported for each graph.  $\text{IC}_{50}$  values were calculated using the least-squares fit of inhibitor concentration versus normalized response in Graph Pad Prism.

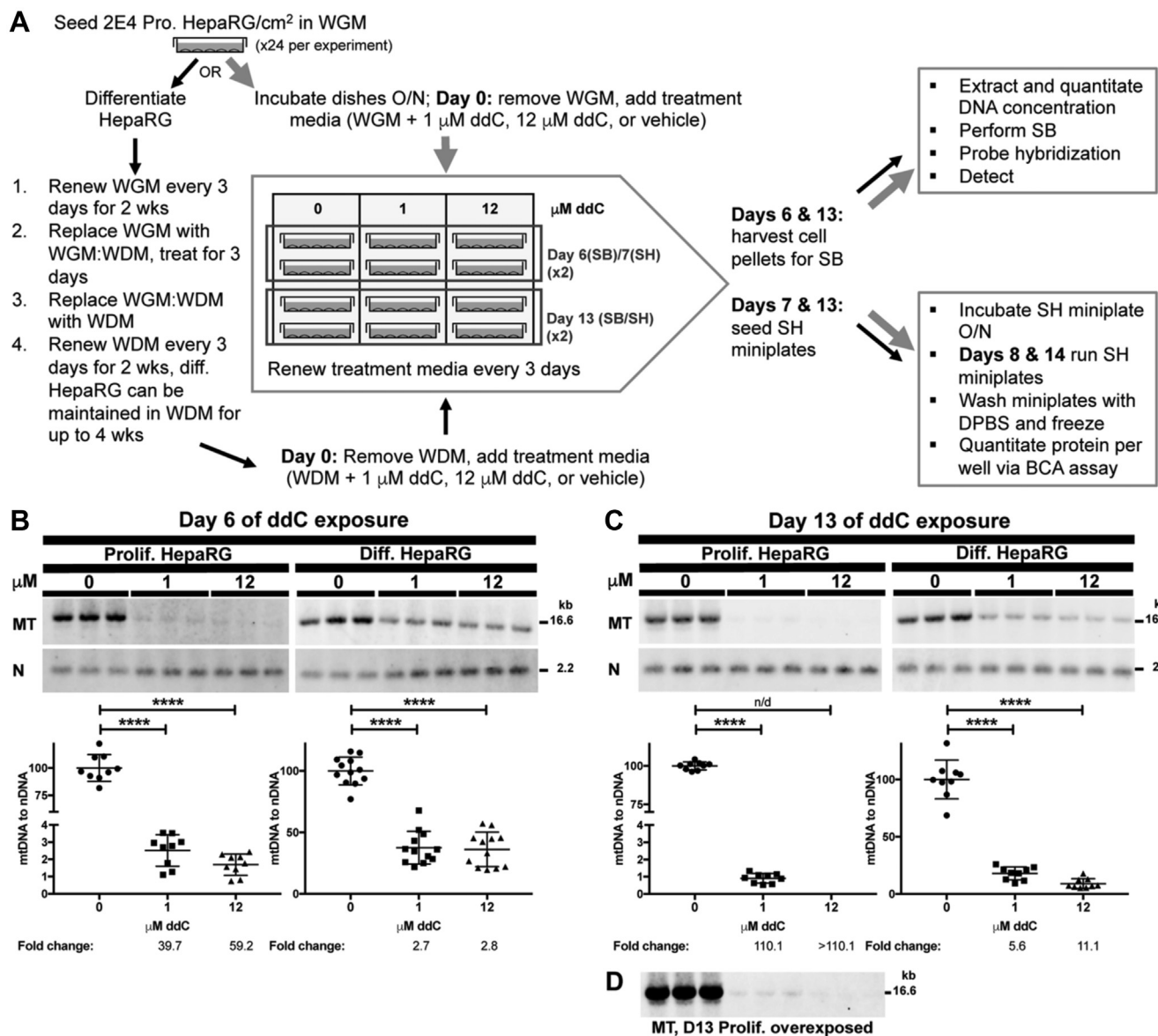


**Figure 3. A greater amount of mitochondrial DNA (mtDNA) depletion is observed in proliferating HepaRG as compared with differentiated HepaRG after 2',3'-dideoxycytidine (ddC) exposure.** A, workflow for seeding, culturing, and exposing HepaRG cells to ddC. Twenty-four tissue culture dishes were seeded with  $2 \times 10^4$  proliferating HepaRG cells/cm<sup>2</sup>, then either subjected to the differentiation protocol (*thin black arrows*) or incubated overnight (O/N), then exposed to ddC on the next day in Working Growth Medium (WGM) (*thick gray arrows*). After the 31-day differentiation process, cells were exposed to ddC in Working Differentiation Medium (WDM), Day 0. For each experiment, one-quarter of the tissue culture dishes were harvested on day 6 post-ddC exposure for Southern blotting (SB) and one-quarter were harvested on day 7 for Seahorse (SH). The remaining half of the tissue culture dishes were harvested on day 13. Experiments were repeated three times with three different cell passages (see [Experimental procedures](#) for details). Southern blots of proliferating and differentiated HepaRG mtDNA content following B, 6 and C, 13 days of ddC exposure. A representative blot is shown for each experiment. Triplicate 1  $\mu$ g reactions of whole-cell DNA extracts were digested with BamHI then loaded and electrophoresed on an agarose gel before blotting and nonradioactive probe hybridization. Except for blots containing samples obtained from proliferating HepaRG at day 13, mtDNA content was measured on blots that were simultaneously probed with the 18S nDNA probe (N) and the mtDNA-specific probe (MT) as described in the legend for [Figure 1](#), and the mean normalized band intensity values of the vehicle control samples (0  $\mu$ M ddC) were set to 100%. Dual-probed blots containing day 13 samples from proliferating HepaRG treated with 1  $\mu$ M could not be quantitated owing to low mtDNA signal; however, when the blots were stripped and probed individually with the mtDNA probe, stripped again, and then probed with the 18S probe, 0 and 1  $\mu$ M mtDNA bands could be quantitated in Fiji as described (79). To confirm equal loading of whole-cell extracted DNA into each lane, the %CV for the nDNA bands on the single-probed 18S blots were at most 11% ( $100\% \pm 11\%$  for 0  $\mu$ M;  $102\% \pm 10\%$  for 1  $\mu$ M;  $101\% \pm 8\%$  for 12  $\mu$ M, errors are SDs), and the 0, 1, and 12  $\mu$ M ddC-treated 18S sample band intensities are not significantly different from one another as judged by a one-way ANOVA. Data presented in the graphs are mean  $\pm$  SD,  $n \geq 9$  ( $\geq 3$  blots from three independent experiments using different preparations/passages of cells); statistically significant differences in mtDNA content were determined by ANOVAs except for proliferating HepaRG day 13, which was done by a Welch's *t* test as the 12  $\mu$ M ddC-treated sample had no detectable mtDNA. \*\*\*\**p*  $\leq$  0.0001 between vehicle control (0  $\mu$ M) and 1 or 12  $\mu$ M. D. An overexposed image of proliferating HepaRG day 13 samples with the mtDNA-specific probe (same image as in C). BCA, bicinchoninic acid.

values reported for human THLE-2 liver epithelial cells after 6 days of treatment with ddC,  $1.6 \pm 2$   $\mu$ M (50). In contrast, differentiated HepaRG cells are significantly less sensitive to ddC having an IC<sub>50</sub> of  $22 \pm 1$   $\mu$ M, [Figure 2C](#).

#### Experimental design for determining the effects of ddC on mitochondrial functions

Previous experiments examining the off-target effects of ddC on mitochondrial functions have exploited proliferating

## Utilizing HepaRG to understand ddC mitochondrial toxicity

human cell lines, varying incubation times (3–15 days), and varying concentrations of ddC, *e.g.*, 0.05, 0.5, 5, 10, 20, and 30  $\mu\text{M}$  (3, 11, 14–16, 51, 52). Based on our survival curve experiments, the reported peak concentrations of ddC in plasma, and the chronic months-long dosing periods reported for HIV-infected patients (2), we chose to examine 1 and 12  $\mu\text{M}$  ddC to determine the effects of ddC on proliferating and differentiated HepaRG mtDNA maintenance, cellular viability, and mitochondrial bioenergetics. At time point zero (day 0) ddC was added to either Working Growth Medium (WGM) or Working Differentiation Medium (WDM), then proliferating or differentiated HepaRG cells were exposed to the WGM + ddC or WDM + ddC treatment media, respectively. One quarter of the cells were harvested on day 6 for Southern blot analysis of WCE DNA and one quarter were harvested on day 7 for bioenergetic analysis. The remaining half of the cells were harvested on day 13, Figure 3A.

### Treatment with ddC causes rapid mtDNA depletion in proliferating HepaRG

As a proliferating HepaRG cell contains 2.9-fold less mtDNA than a differentiated cell, we predicted that mtDNA depletion would be more severe for proliferating cells following exposure to ddC. Southern blotting demonstrated extreme depletion of proliferating HepaRG mtDNA relative to nDNA for both 1 and 12  $\mu\text{M}$  ddC-treated cells at 6 and 13 days post-treatment, Figure 3, B–C. Relative to untreated control cells, after 6 days of exposure to 1 and 12  $\mu\text{M}$  ddC proliferating HepaRG retained only 2.5% and 1.7% mtDNA, respectively, Figure 3B. After 13 days of exposure to 12  $\mu\text{M}$  ddC, mtDNA levels were so low that they could not be measured, Figure 3, C–D. And, after 13 days of exposure to 1  $\mu\text{M}$  ddC, mtDNA levels dropped to 0.9% of untreated HepaRG mtDNA levels. These data support that proliferating HepaRG mtDNA is sensitive to rapid depletion upon exposure to ddC.

### Treatment with ddC causes slower mtDNA depletion in differentiated HepaRG

Southern blotting revealed that ddC treatment caused a slower rate of mtDNA depletion in differentiated HepaRG relative to proliferating cells, Figure 3, B–C. Relative to untreated control cells, after 6 days of exposure to 1 and 12  $\mu\text{M}$  ddC, differentiated cells harbored 37% and 36% of untreated HepaRG mtDNA levels, respectively, Figure 3B. After 13 days, mtDNA levels fell to 18% and 9% for 1 and 12  $\mu\text{M}$  ddC-treated cells, respectively, Figure 3C. Based on these data, we estimate mtDNA depletion due to ddC exposure to occur 15 $\times$  to 21 $\times$  faster in proliferating *versus* differentiated HepaRG (*e.g.*, for differentiated to proliferating HepaRG at 1  $\mu\text{M}$  ddC day 6, 37%/2.5% = 15). If differentiated cells did not undergo mtDNA replication, then one would expect that ddC treatment would not affect mtDNA copy number; thus, these data support the concept that mtDNA replicates independently from the cell cycle in quiescent and nonreplicating postmitotic cells (41–45).

### Only proliferating HepaRG viability is reduced following a 13-day ddC exposure

Proliferating and differentiated HepaRG cell counts and viability were measured on days 7 and 13 post-ddC exposure utilizing the trypan blue exclusion method. Proliferating HepaRG cells displayed reductions in the number of viable cells remaining on cell culture dishes that correlated with increasing ddC concentration and treatment time, Figure 4. In comparison with vehicle control-treated viable cell counts (100%), by exposure day 7, 73.4% and 55.8% of the 1 and 12  $\mu\text{M}$  ddC-treated viable cells remained on the dishes, respectively. Six days later (day 13 post-ddC exposure), the cell counts were 47.4% and 39.1% of the control cell counts for the 1 and 12  $\mu\text{M}$  ddC-treated proliferating cells, respectively. The viability of the proliferating cell population remaining on the culture dishes remained high ( $\geq 94\%$ ) for proliferating cells treated with 0, 1, and 12  $\mu\text{M}$  ddC over 7 days. However, at 13 days post-treatment relative to control-treated cells, the viability of the remaining cells on the dish for 1 and 12  $\mu\text{M}$  ddC treatments decreased to 86% and 85%. Simply put, proliferating HepaRG cell counts and viability deteriorated with lengthier ddC exposure. In contrast, differentiated cells maintained vehicle control levels of percent viability at both concentrations of ddC and at both time points. Differentiated HepaRG cells exposed to 1 and 12  $\mu\text{M}$  ddC displayed trends of slight reductions in the number of viable cells remaining on cell culture dishes; however, these trends were not significantly different from vehicle control-treated cell counts, Figure 4.

### Exposure to ddC causes severe deterioration of proliferating HepaRG bioenergetics

To determine mitochondrial bioenergetic profiles, cells were exposed to known pharmacological stressors of the OXPHOS machinery. Mitochondrial OXPHOS is the  $\text{O}_2$ -dependent process of coupling substrate oxidation to the production of the energy-rich molecule adenosine triphosphate (ATP). During OXPHOS, molecular  $\text{O}_2$  is reduced to water ( $\text{H}_2\text{O}$ ). An XFp  $\text{O}_2$  biosensor measures the real-time rate at which cells convert  $\text{O}_2$  to  $\text{H}_2\text{O}$ , the  $\text{O}_2$  consumption rate (OCR). A second XFp biosensor measures the extracellular acidification rate (ECAR) resulting from the cytoplasmic breakdown of glucose-derived pyruvate to lactate and the respiratory evolution of carbon dioxide ( $\text{CO}_2$ ). Glycolysis is the major cytosolic  $\text{O}_2$ -independent metabolic pathway that converts one molecule of glucose into two molecules of pyruvate, ATP, and NADH. When pyruvate is shunted through the mitochondrion to the pyruvate dehydrogenase complex and subsequently through the tricarboxylic acid cycle,  $\text{CO}_2$  is generated. In solution, a molecule of  $\text{CO}_2$  can combine with a molecule of  $\text{H}_2\text{O}$  forming carbonic acid that dissociates at physiological pH into the bicarbonate anion and a proton that contributes to medium acidification (53).

To determine the effects of ddC on HepaRG bioenergetic profiles, Mito Stress tests were conducted using the Seahorse XFp. Oligomycin, FCCP, and rotenone plus antimycin A were sequentially injected during the experiments, Figure 5 A.

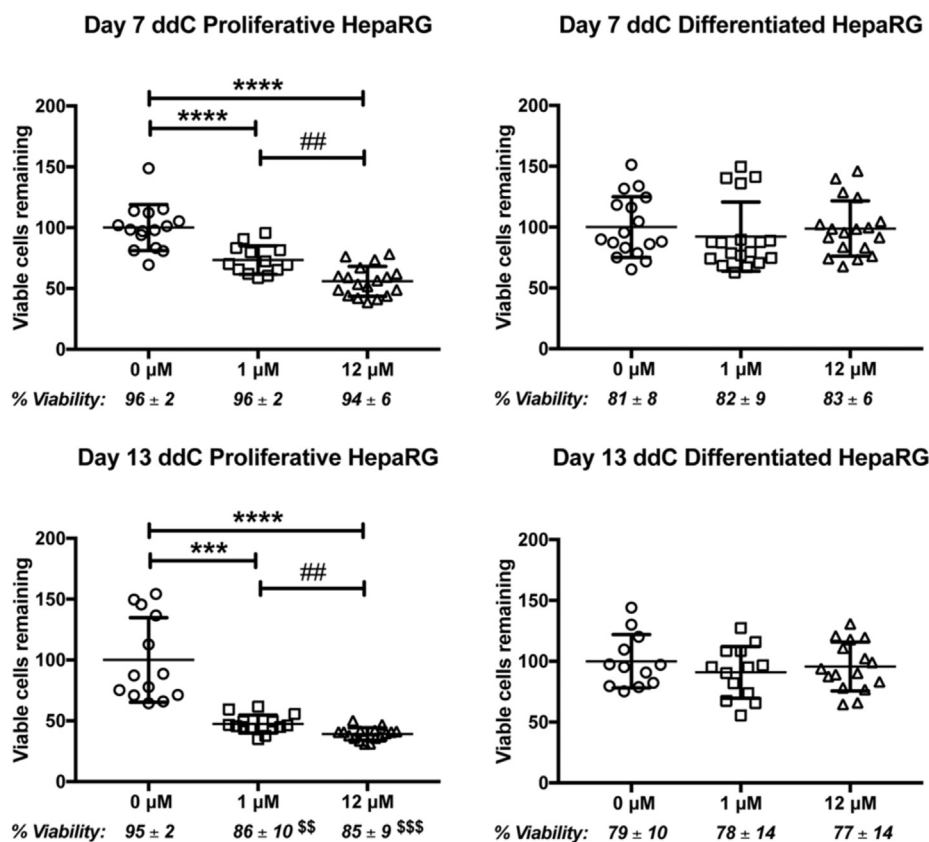


**Figure 4. HepaRG viable cell counts following 2',3'-dideoxycytidine (ddC) exposure.** HepaRG cells were exposed to vehicle, 1, or 12  $\mu\text{M}$  ddC for 7 and 13 days, then cells were counted. The number of viable cells remaining on the cell culture dishes was determined utilizing the trypan blue exclusion method. In each set of experiments, the vehicle control-treated (0  $\mu\text{M}$  ddC) cell counts were set to 100 (%). Data are presented as mean viable cell counts  $\pm$ SD,  $n \geq 12$  ( $\geq$ quadruplicate from three independent experiments using different cell passages). The percentage of the viable (clear) cells of the total remaining cell population (blue and clear) is reported under the graphs as percent viability. The statistical significance was determined by one-way ANOVA for parametric data and by Kruskal–Wallis tests for nonparametric data. \*\*\*\* $p \leq 0.0001$  between vehicle control (0  $\mu\text{M}$ ) and 1 or 12  $\mu\text{M}$ ; \*\*\* $p \leq 0.001$  between 0 and 1  $\mu\text{M}$ ; ## $p \leq 0.01$  between 1 and 12  $\mu\text{M}$ .

Rotenone and antimycin A are inhibitors of OXPHOS complexes I and III, respectively, and were the last stressors added during the experiments to terminate electron flow through the electron transport chain and to enable the calculation of oxygen consumption from nonmitochondrial oxidases. This *nonmitochondrial respiration* parameter represents cellular OCR remaining following rotenone plus antimycin A treatment (see Fig. S1). The *basal respiration* parameter is the difference between the OCR measured just before oligomycin injection and the nonmitochondrial respiration parameter. Basal respiration represents the sum of the respiration used to power ATP production and respiration associated with proton leakage across the inner membrane. Following the injection of oligomycin to inhibit complex V, ATP production slows and respiration utilized to power ATP production decreases. The amount of basal OCR sensitive to oligomycin represents a measurement of *ATP-linked respiration* (53). After subtracting the nonmitochondrial respiration rate, FCCP stimulation of OCR provides a measurement of the *maximal respiratory capacity* of cells and by extension the maximal capacity to oxidize substrates *via* the OXPHOS machinery. Next, the difference between the maximal respiratory capacity and basal respiration was used to calculate the *spare respiratory capacity*.

Spare respiratory capacity is defined as the extramitochondrial capacity available to produce ATP during stress or increased work. The spare respiratory capacity is suggested to be important for cellular function and long-term survival (54). During substrate oxidation, a portion of the proton motive force is not utilized to drive ATP synthesis *via* complex V, and some protons “leak” back into the matrix *via* inducible uncoupling proteins and through the presence (not the activity) of the inner membrane adenine nucleotide translocase, ANT (55). This *proton leak-linked respiration* parameter is the remaining mitochondrial respiration detected in the presence of oligomycin.

We examined the effects of cell type (proliferating or differentiated), time (day 8 or 14), and ddC concentration (0, 1, and 12  $\mu\text{M}$ ) on bioenergetic parameters. We begin by describing proliferating cell results and highlight the OCR and ECAR profiles following 8 days of 0, 1, or 12  $\mu\text{M}$  ddC exposure to illustrate the effect of the NRTI on HepaRG OCRs and by extension mitochondrial function, Figure 5A. The effects of day 8 and 14 ddC exposures on proliferating and differentiated HepaRG bioenergetic parameters are shown in Figure 5B.

Proliferating HepaRG mitochondria were sensitive to 8-day ddC exposures. Following the 1 and 12  $\mu\text{M}$  ddC treatments

## Utilizing HepaRG to understand ddC mitochondrial toxicity

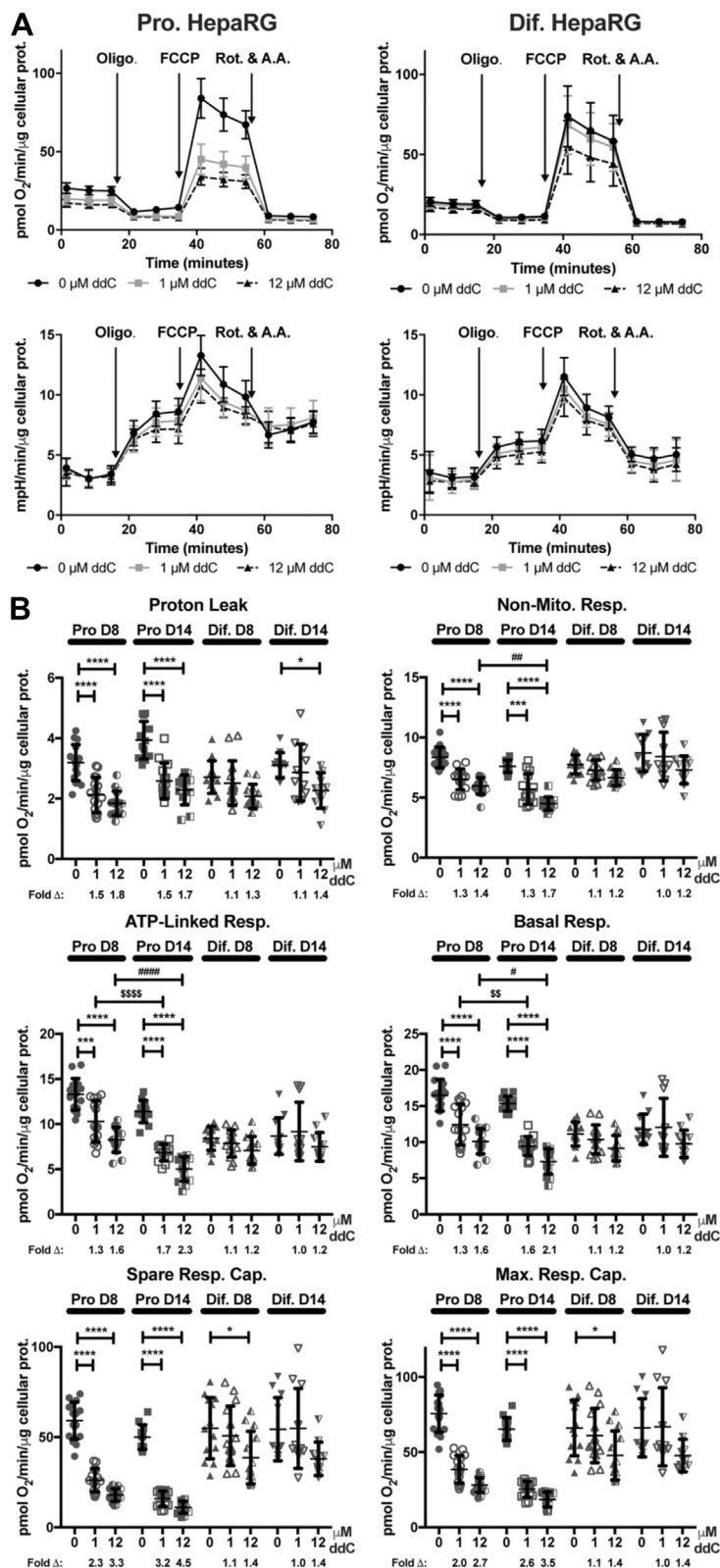


**Figure 5. Exposure to 2',3'-dideoxycytidine (ddC) causes aberrant bioenergetics in proliferating and differentiated HepaRG cells.** A, proliferating (Pro.) and differentiated (Dif.) HepaRG Mito Stress test oxygen consumption rates (pmol O<sub>2</sub>/min/μg cellular protein) and extracellular acidification rates (mpH/min/μg cellular protein) following 8 days of treatment with 0, 1, or 12 μM ddC. Metabolic stressors were injected sequentially from Ports a (2 μM oligomycin final well concentration), b (1 μM FCCP final well concentration), and c (0.5 μM antimycin A + 0.5 μM rotenone, final well concentrations). A.A., antimycin A; Oligo., oligomycin; Rot., rotenone. Data are mean values ± SD; n ≥ 12, ≥quaduplicate from three independent experiments using different preparations/passages of cells. B, scatter dot plots of proliferating and differentiated HepaRG mitochondrial bioenergetic parameters following 8 and 14 days of ddC exposure. Bioenergetic parameters: Proton Leak, and nonmitochondrial respiration (Non-Mito Resp.), ATP-linked respiration (ATP-linked Resp.), basal respiration (Basal Resp.), spare respiratory capacity (Spare Resp. Cap.), and maximal respiratory capacity (Max. Resp. Cap.). Data are presented

proliferating cells had the greatest defects in spare and maximal respiratory capacities, Figure 5B. For 1  $\mu\text{M}$  ddC-treated cells, spare respiratory and maximal respiratory capacities were 2.3- and 2.0-fold reduced from vehicle control-treated cells, respectively. For 12  $\mu\text{M}$  ddC-treated proliferating cells, spare and maximal respiratory capacities were 3.3- and 2.7-fold reduced. For 1  $\mu\text{M}$  ddC-treated cells, proton leak-linked respiration was reduced 1.5-fold and nonmitochondrial respiration, basal respiration, and ATP-linked respiration were the least changed of the various parameters having 1.3-fold reductions from vehicle control; however, these changes are all significantly different. Similar trends were noted for 12  $\mu\text{M}$  treated cells with greatest defects ranging from spare respiratory capacity (3.3-fold) > maximal respiratory capacity (2.7-fold) > proton leak-linked respiration (1.8-fold) > ATP-linked respiration (1.6-fold) = basal respiration (1.6-fold) > nonmitochondrial respiration (1.4-fold reduced from control).

After six more days of ddC exposure (day 14 post-treatment) proliferating HepaRG bioenergetic parameters including basal, ATP-linked, and nonmitochondrial respiration continued to crash, Figure 5B. Significant differences in day 8 versus day 14 basal and ATP-linked respirations were observed between cells treated with both 1 and 12  $\mu\text{M}$  ddC. Compared with control-treated cells, the basal respiration for 1 and 12  $\mu\text{M}$  ddC treatments dropped from 1.3- and 1.6-fold on day 8 to 1.6- and 2.1-fold reductions on day 14, respectively. Likewise, the ATP-linked respiration for 1 and 12  $\mu\text{M}$  ddC-treated cells fell from 1.3- and 1.6-fold on day 8 to 1.7- and 2.3-fold on day 14. For nonmitochondrial respiration, only the 12  $\mu\text{M}$  treated samples were significantly different between days 8 and 14 decreasing from 1.4- to 1.7-fold, respectively.

Similar to what was observed at 8 days post-treatment, after 14 days of ddC exposure the 1 and 12  $\mu\text{M}$  treated proliferating cells had the greatest defects (fold-changes) in spare and maximal respiratory capacities. For 1  $\mu\text{M}$  ddC-treated cells, spare and maximal respiratory capacities were 3.2- and 2.6-fold reduced from vehicle control-treated cells, respectively. For 1  $\mu\text{M}$  ddC-treated cells, proton leak-linked and nonmitochondrial respiration were decreased by 1.5- and 1.3-fold, respectively. The range of bioenergetic defects for 12  $\mu\text{M}$  treated cells at day 14 from highest to lowest were spare respiratory capacity (4.5-fold) > maximal respiratory capacity (3.5-fold) > ATP-linked respiration (2.3-fold) > basal respiration (2.1-fold) > proton leak-linked respiration (1.7-fold) = nonmitochondrial respiration (1.7-fold reduced from control).

#### Exposure to ddC causes milder deterioration of differentiated HepaRG bioenergetics

Although several differentiated HepaRG bioenergetic parameters were slightly reduced upon 1  $\mu\text{M}$  ddC treatment

following 8 and 14 days of exposure (day 8: proton leak, basal respiration, and nonmitochondrial respiration; day 14: proton leak) these changes, as well as the other bioenergetic parameters, were not significantly different from control-treated cells, Figure 5B. Similarly, upon 12  $\mu\text{M}$  ddC treatment following 8 and 14 days of exposure many parameters were slightly reduced but the decreases were not significant (day 8: proton leak, ATP-linked respiration, basal respiration, nonmitochondrial respiration; day 14: spare respiratory capacity, maximal respiratory capacity, ATP-linked respiration, basal respiration, nonmitochondrial respiration). Significant changes were observed for 12  $\mu\text{M}$  ddC treatments at day 8 including spare respiratory and maximal respiratory capacities. Both capacities were 1.4-fold reduced from control-treated cells. Finally, by day 14, 12  $\mu\text{M}$  ddC-treated differentiated cell proton leak-linked respiration was 1.4-fold reduced from control-treated cells, Figure 5B. Taken together with the mtDNA depletion, percent viability, and chronic/long-term treatment of patients with NRTIs, these results emphasize the importance of understanding the antiviral off-target effects on mitochondrial functions in different cell types.

#### Discussion

Recently, Southern blotting served as a powerful tool to characterize and identify the human degradosome, the mitochondrial machinery that degrades mtDNA (56). In the degradosome model, the p140 catalytic subunit of Poly harboring the 3'-5' exonuclease activity, the 5'-3' mtDNA Twinkle helicase, and the 5'-3' exonuclease MGME1 work in concert to quickly degrade linear mtDNA molecules. We predict that mtDNA genome instability in nonproliferating differentiated cells is initiated *via* ddC-stalled replisomes. In this scenario, the mtDNA degradosome machinery degrades partially synthesized and stalled nascent strands and broken mtDNA strands leading to mtDNA depletion and loss of mitochondrial bioenergetics. Based on our quantitative analysis of 7400 mtDNA molecules per differentiated HepaRG cell (Fig. 1) and assuming a steady-state rate of mtDNA synthesis and degradation in noncycling cells, we estimate that, on the 13th day of 12  $\mu\text{M}$  ddC exposure the 9% level of mtDNA (11.1-fold, Fig. 3C) represents  $\sim 700$  mtDNA molecules per cell. This represents a loss of  $\sim 22$  mtDNA molecules per hour (depletion of  $7400 - 700 = 6700$  molecules over  $312 \text{ h} = \sim 22$ ). By the eighth day of 12  $\mu\text{M}$  ddC treatment, the differentiated HepaRG spare respiratory and maximal respiratory capacity bioenergetic parameters were slightly but significantly reduced compared with control cells, Figure 5B. These reductions are predicted to weaken the ability of differentiated cells to respond to increased energy demands and to withstand stressful conditions (53). Likewise, following 14 days of 12  $\mu\text{M}$  ddC treatment, proton leak-linked respiration was reduced

with mean values and SD errors on the plots,  $n \geq 11$  (greater than triplicate from three independent experiments using different passages). The fold-changes ( $\Delta$ ) of 0  $\mu\text{M}$  ddC (control)-treated bioenergetic parameters relative to 12 and 1  $\mu\text{M}$  ddC-treated cells are listed under each plot. The statistical significance was determined by three-way ANOVA. \*\*\*\* $p \leq 0.0001$ , 0 versus 1 or 12  $\mu\text{M}$ ; \*\*\* $p \leq 0.001$ , 0 versus 1  $\mu\text{M}$ ; \* $p \leq 0.05$ , 0 versus 12  $\mu\text{M}$ ; \$\$\$ $p \leq 0.0001$ , D8 versus D14 at 1  $\mu\text{M}$ ; \$\$ $p \leq 0.01$ , D8 versus D14 at 1  $\mu\text{M}$ ; ##### $p \leq 0.0001$ , D8 versus D14 at 12  $\mu\text{M}$ ; ## $p \leq 0.01$ , D8 versus D14 at 12  $\mu\text{M}$ ; # $p \leq 0.05$ , D8 versus D14 at 12  $\mu\text{M}$ . The  $p$ -values for differentiated HepaRG spare respiratory and maximal respiratory capacities on day 14 post-treatment with 12  $\mu\text{M}$  ddC were 0.07 and 0.09, respectively. Bioenergetic parameters were calculated as previously described (31).

## Utilizing HepaRG to understand ddC mitochondrial toxicity

1.4-fold. Thus, the results of this study support that mitochondrial genotoxic agents impair nonproliferating cell mitochondrial functions. Several proteins associate with mtDNA at distinct nucleoid structures on the matrix-side of the mitochondrial inner membrane (MIM) (57). Mitochondrial nucleoids occur at specific voids between mitochondrial cristae (58) suggesting mtDNA-containing nucleoids could provide a structural role at the MIM that is necessary for the proper function of membrane proteins. As some protons leak back into the matrix *via* the MIM-localized ANT, and ANT2 (*SLC25A5*) and ANT3 (*SLC25A6*) have been identified as human mtDNA nucleoid proteins (55, 59), we predict that ddC-induced mtDNA depletion in differentiated HepaRG could alter the structure of the MIM and the MIM-localized ANT gated pores resulting in decreased proton leakage through aberrant pores.

Human cell culture studies have shown that exposure to ddC causes depletion of mtDNA-encoded OXPHOS subunits necessary for mitochondrial functions. In a 5-day ddC exposure study using PC-3 cells treated with different concentrations of the drug, exposure to 1  $\mu\text{M}$  ddC caused a decline in the levels of the mtDNA-encoded COX1 protein down to 20% of vehicle control-treated samples. In contrast, the levels of the nDNA-encoded succinate dehydrogenase remained high at  $\sim 85\%$  of control-treated samples (60). Furthermore, Le Guillou *et al.* (61) recently demonstrated that a 2-week treatment of differentiated HepaRG with 20  $\mu\text{M}$  ddC caused decreases in the levels of mtDNA and mtDNA-encoded ND1 and COX2 polypeptides but not in the amount of the nDNA-encoded COX4 polypeptide. Guillou *et al.* used quantitative PCR to detect differentiated HepaRG mtDNA levels that were reduced to  $\sim 10\%$  of untreated control levels, which is in good agreement with our results following 13 days of 12  $\mu\text{M}$  ddC treatment, Figure 3C. Therefore, as mammalian mtDNA replication (and degradation/turnover) is independent of the cell cycle, the resulting ddC-induced bioenergetic impairments that we observed in differentiated (and undifferentiated) HepaRG likely result from insufficient mtDNA-encoded OXPHOS components, Figure 6. Maintaining the function of terminally differentiated cells in organs and tissues of patients chronically administered NRTIs is of concern as nonproliferating differentiated HepaRG suffered increased mtDNA depletion with increased treatment times; compare differentiated HepaRG mtDNA content in Figure 3, B–C. Although 13-day ddC treatments did not result in statistically significant differences in differentiated HepaRG cellular viability, proton leak-linked respiration was decreased by day 14. On the other hand, when differentiated HepaRG cells were treated with 0.25  $\mu\text{M}$  ddC (and up to 128  $\mu\text{M}$  ddC) for 15 days, cellular viabilities significantly decreased compared with vehicle control-treated cells, Figure 2C (e.g., 78% and 52% viability for 1 and 8  $\mu\text{M}$  ddC-treated cells respectively,  $p < 0.0001$  for both by one-way ANOVA). Taken together with the observations that 1) exposure to 12  $\mu\text{M}$  ddC for 13 days caused less damage to proliferating cells as compared with a 15-day 8  $\mu\text{M}$  ddC exposure (39% versus 6% viable cells remaining, respectively, compare Figures 4 and 2B) and that 2) proliferating cell

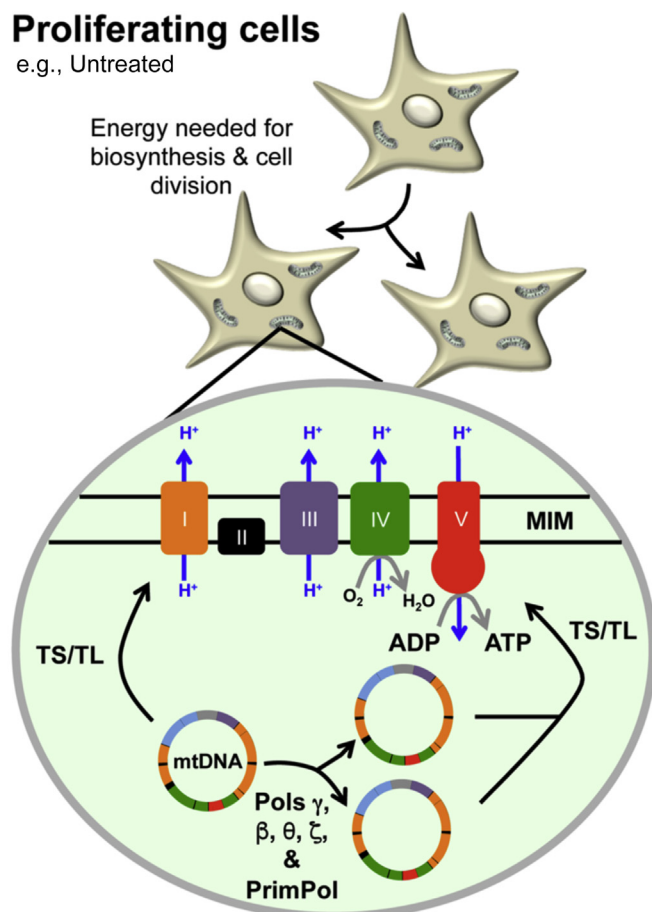
ATP-linked, basal, and nonmitochondrial respiration parameters were further altered/decreased at day 14 of ddC exposure as compared with day 8 (Fig. 5), we conclude that longer exposures to a mtDNA toxicant exacerbate mitochondrial damage in both proliferating and differentiated cells. An increased ddC exposure time would likely cause further mtDNA depletion and deterioration of bioenergetic functions in differentiated cells. The negative effects of long-term ddC treatment on postmitotic cell mitochondrial functions are particularly concerning for neuron and glia cells as ddC has been demonstrated to penetrate the blood–brain barrier in rats (49). Our results also raise concern regarding the health and regeneration of liver tissue when exposed to mitotoxic agents as the liver regeneration process has been proposed to involve both proliferating liver stem/progenitor cells and differentiated hepatocytes (62).

We found extreme defects in proliferating HepaRG cell mtDNA maintenance and bioenergetics associated with ddC exposure. After 6 days of ddC treatment, proliferating HepaRG mtDNA levels quickly plummeted to  $\leq 2.5\%$  of vehicle control-treated levels. Based on our quantitative analysis of mtDNA molecules per proliferating cell (2600, Fig. 1) and assuming a steady-state rate of mtDNA synthesis and degradation in cycling cells, we estimated that a level of 2.5% would be equal to 65 mtDNAs per cell. Assuming cell growth is not inhibited by ddC, and based on the calculated doubling time of 44 h (Fig. 2), if mtDNA molecules were simply depleted during cell division, then the levels would be  $\sim 6.25\%$  of the starting levels after  $\sim 1$  week of growth in ddC or 163 mtDNAs. A decrease to 6.25% is 2.5- and  $\sim 4$ -fold higher than what was observed following 6 days of treatment with 1 and 12  $\mu\text{M}$  ddC, respectively, Figure 3. Furthermore, proliferating cell growth was inhibited by exposure to 1 and 12  $\mu\text{M}$  ddC as viable cell counts remaining on the culture dishes on day 7 were 73.4% and 55.8% of the control-treated cells, respectively, Figure 4. These data suggest that, in proliferating cells exposed to ddC, simple mtDNA dilution by cell division is not the only mechanism contributing to the loss of mtDNA. In this scenario, we predict that the mitochondrial degradosome plays an active role in mtDNA degradation in proliferating cells as it is in differentiated HepaRG. Perhaps the expression of degradosome subunits is upregulated in undifferentiated proliferating HepaRG causing enhanced mtDNA depletion relative to differentiated cells. By day 8 of ddC treatment, proliferating HepaRG mitochondrial bioenergetic failure was evident. Following 13 days of ddC exposure, mtDNA levels were  $\leq 0.9\%$  and growth and viability were significantly reduced. We predict that by this point in time the intrinsic apoptotic pathway has been activated. By day 14 of ddC exposure proliferating HepaRG basal and ATP-linked respiration parameters crashed, indicating severe mitochondrial bioenergetic failure.

Another explanation for exposure to ddC causing enhanced mtDNA depletion in proliferating HepaRG is that proliferating cells may have decreased drug resistance relative to differentiated cells. Differentiated HepaRG was demonstrated to express multidrug resistance-associated proteins including P-glycoprotein (*ABCB1*), MRP2 (*ABCC2*), and MRP3 (*ABCC3*), (63).

**Proliferating cells**

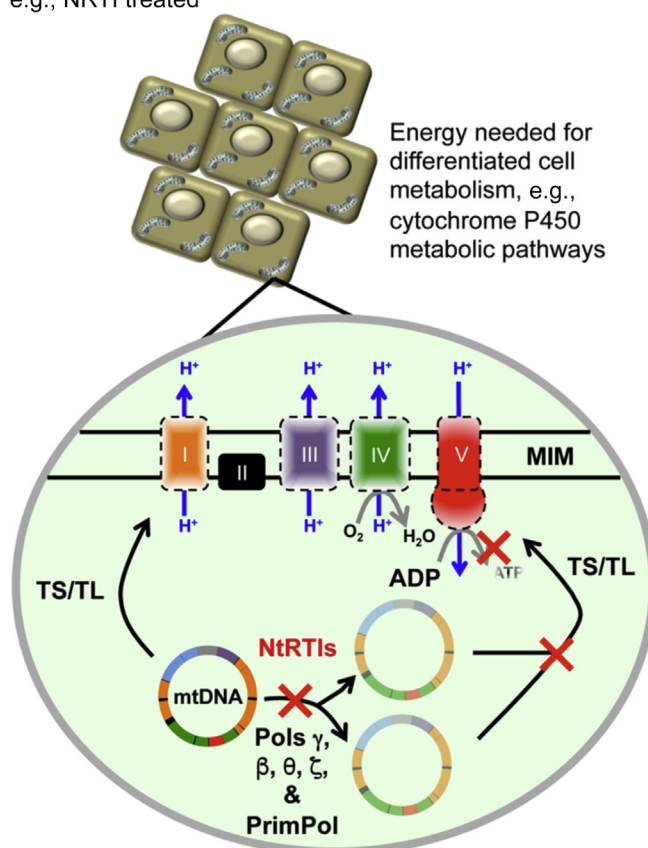
e.g., Untreated

Energy needed for  
biosynthesis & cell  
division

e.g., Untreated mitochondria

**Differentiated cells**

e.g., NRTI treated

Energy needed for  
differentiated cell  
metabolism, e.g.,  
cytochrome P450  
metabolic pathways

e.g., NRTI treated mitochondria

**Figure 6. Mitochondrial DNA (mtDNA) replication occurs in proliferating and differentiated cells.** Nucleoside reverse-transcriptase inhibitors (NRTIs) are metabolically activated by intracellular kinases to nucleotide reverse transcriptase inhibitors (NtRTIs). The insets highlight the mitochondrial matrix, the location of the DNA polymerases, and the mtDNA genome encoding 13 polypeptides of the oxidative phosphorylation (OXPHOS) machinery. The mtDNA genes are colored by OXPHOS complex, orange, purple, green, and red. Orange, OXPHOS complex I (NADH dehydrogenase); black, OXPHOS complex II (succinate dehydrogenase); purple, OXPHOS complex III (cytochrome bc1 complex); green, OXPHOS complex IV (cytochrome c oxidase); red, OXPHOS complex V (ATP synthase). The OXPHOS machinery is localized within the mitochondrial inner membrane (MIM). Within the mitochondrion, NtRTIs compete with native nucleotides at DNA polymerase active sites to inhibit mtDNA replication through chain termination and persistence in the mtDNA genome. H<sup>+</sup>, proton; O<sub>2</sub>, oxygen; H<sub>2</sub>O, water; ADP, adenosine diphosphate; ATP, adenosine triphosphate; TS, mitochondrial transcription; TL, mitochondrial translation; DNA polymerases gamma (Poly), beta (Polβ), theta (Polθ), zeta (Polζ), and PrimPol. See the text for details.

These ATP-binding cassette (ABC) proteins function as ATP-dependent efflux pumps, which export drugs from the cell. In comparison with a CEM human lymphoblastoid cell line expressing low levels of P-glycoprotein, a CEM cell line expressing high levels of P-glycoprotein was demonstrated to be less effective at inhibiting HIV replication in the presence of AZT (64). Also, CEM cells that are resistant to the acyclic nucleoside phosphonate analog 9-(2-phosphonyl-methoxyethyl)adenine (PMEA, adefovir) were demonstrated to overexpress MRP4 (*ABCC4*), and MRP4 overexpression impaired the antiviral efficacy of PMEA and AZT-MP and correlated with the ATP-dependent efflux of the analogs (65). In a follow-up study, the PMEA-resistant cell line was used to show that MRP4 can mediate active cellular efflux of tenofovir in comparison with its PMEA-sensitive parental CEM cell line (66). In addition to the increased expression of degradosome gene products or downregulation of a ddC efflux pump, other possible mechanisms for enhanced mtDNA degradation in

proliferating cells could include increased mitophagy (autophagic degradation of damaged mitochondria) or increased degradosome activity. We predict that lower concentrations of mitochondrial dNTPs in proliferating cell mitochondria could signal a switch between the p140 catalytic subunit DNA polymerase and exonuclease activities as *in vitro* the proofreading exonuclease activity of p140 degrades linear DNA in the absence of dNTPs (67). Whatever the mechanism, it is clear that future work is needed to understand how the molecular machinery regulating mtDNA homeostasis in proliferating and differentiated cells influences cellular susceptibility to mtDNA toxicants such as ddC.

In summary, we have shown that human proliferating and differentiated HepaRG cells are excellent model systems to study the harmful effects of a mitochondrial genotoxic agent, the antiretroviral ddC. The results of this study demonstrate the importance of carefully considering the off-target effects of a drug on both proliferating and differentiated cell

## Utilizing HepaRG to understand ddC mitochondrial toxicity

mitochondrial functions. Caution needs to be taken when attempting to study drugs that inhibit proliferating cancer cell mtDNA replication as we have shown that nonproliferating differentiated HepaRG mtDNA genomes and mitochondrial bioenergetics are sensitive to ddC exposure. It is important to note that the mtDNA depletion observed in this study occurred in just under 2 weeks but patients treated with NRTIs are chronically exposed to drugs. We expect that the long-term exposure to mtDNA toxicants will be harmful to both proliferating and nonproliferating cell mitochondria *in vivo*. Awareness about the toxic effect of drugs and pollutants on mitochondrial function is rapidly accelerating (19, 68–70). For example, hepatitis C virus ribonucleoside analogs designed to inhibit viral RNA synthesis have been demonstrated to have off-target effects on the human mitochondrial RNA polymerase, POLRMT (71). POLRMT is a dual-purpose enzyme required for priming mtDNA replication and for carrying out mitochondrial-specific transcription. Another example is the polycyclic aromatic hydrocarbon benzo(a)pyrene, which causes more damage to mtDNA than to nDNA (20). Further complicating mitochondrial toxicity, genetic mutations encoding variants of DNA polymerase subunits, which localize to the mitochondrion, could predispose patients to mitochondrial toxicity, e.g., p140 (R964C, R953C, and E1143D/G) and PrimPol D114N (72–77). Although we have characterized the differential effects of a single NRTI on proliferating and differentiated HepaRG in this work, other antivirals, drugs, or environmental mitochondrial toxicants should be investigated in the future. As both proliferating and differentiated HepaRG are affected by ddC treatment, this study emphasizes that different cell types need to be taken into account when determining the off-target effects of environmental toxicants or drugs on mitochondrial function.

### Experimental procedures

#### HepaRG cell culture and differentiation

The proliferating HepaRG hepatoma-derived cell line was purchased from Biopredic International (Saint-Grégoire, France). Cells were cultured and differentiated according to Biopredic International standard operating procedure and as described (25, 28, 31). Briefly, proliferating HepaRG were grown in Working Growth Medium (WGM) consisting of William's E Medium (Thermo Fisher Scientific), 2 mM GlutaMAX (Thermo Fisher Scientific) with the addition of HepaRG Growth Medium Supplement (Lonza). Cells were grown at 37 °C and 5% CO<sub>2</sub> in a humidified incubator, and the medium was refreshed every 3 days. For the day-to-day examination of cell culture, a Leica DMi1 inverted microscope with 10× and 20× phase contrast objectives was used. Proliferating HepaRG cells were passaged between days 12 and 15 post-seeding by washing with prewarmed Dulbecco's phosphate-buffered saline (DPBS) followed by gentle trypsinization and neutralization with prewarmed WGM. Tissue culture dishes were seeded with 2 × 10<sup>4</sup> proliferating cells/cm<sup>2</sup> and cells were not passaged more than 18 times, P18. The Working Differentiation Medium (WDM) consisted of William's E Medium

(Thermo Fisher Scientific), 2 mM GlutaMAX (Thermo Fisher Scientific), with the addition of HepaRG Differentiation Medium Supplement (Lonza). The differentiation process was started 2 weeks after passaging proliferating HepaRG cells. The WGM was replaced with Combination Medium (CM), consisting of a 1:1 mixture of WGM to WDM, and 3 days later the CM was replaced with WDM. The medium was renewed every 3 days for 2 weeks and after 2 weeks cells attained differentiated hepatocyte-like morphology (see Fig. 1A for a timeline of HepaRG differentiation). Following treatment with prewarmed trypsin and neutralization with prewarmed medium, HepaRG viable cell counts were determined utilizing the trypan blue exclusion method.

#### Determining ddC IC<sub>50</sub> values

The HepaRG cytotoxic effect of ddC was initially estimated *via* percent growth inhibition relative to untreated control cells. This effect is expressed as the half-maximal inhibitory concentration (IC<sub>50</sub>) or concentration of ddC that reduces the number of viable treated cells by 50% relative to untreated control cells. The day before drug exposure, proliferating HepaRG cells were seeded at 2 × 10<sup>4</sup> cells/cm<sup>2</sup> in Falcon 24-well flat-bottom tissue culture plate wells and grown at 37 °C, 5% CO<sub>2</sub> in a humidified incubator. On the next day, cells in triplicate wells were exposed to WGM treatment media containing 128, 8, 4, 2, 1, 0.5, 0.25, or 0 μM ddC for 15 days, and the treatment media were refreshed every 3 days. On the day of counting, treatment media were removed and the viable cells remaining in triplicate wells were washed with DPBS, trypsinized, neutralized with their respective treatment medium, and then counted using trypan blue. Untreated cell counts (0 μM ddC) were set to 100% and the IC<sub>50</sub> values were calculated in Prism 7 using nonlinear regression analysis, the least-squares fit of inhibitor concentration *versus* normalized response. For the differentiated HepaRG experiment, proliferating HepaRG cells were seeded at 2 × 10<sup>4</sup> cells/cm<sup>2</sup> in Falcon 24-well flat-bottom tissue culture plate wells and subjected to the differentiation protocol as described above. Following the differentiation process, cells in triplicate wells were exposed to WDM treatment media containing 128, 8, 4, 2, 1, 0.5, 0.25, or 0 μM ddC for 15 days, and treatment media were refreshed every 3 days. Viable differentiated cells were counted and IC<sub>50</sub> values were calculated as described above for proliferating HepaRG.

#### ddC treatment of proliferating HepaRG for whole-cell DNA extraction

Proliferating HepaRG in WGM were seeded at 2 × 10<sup>4</sup> cells/cm<sup>2</sup> and allowed to adhere to the bottom of cell culture dishes overnight at 37 °C, 5% CO<sub>2</sub> in a humidified incubator. Treatment media were prepared by adding ddC to a final concentration of 0 (vehicle treated), 1, or 12 μM in WGM. On the next day, WGM from the cell culture dishes was replaced with WGM + vehicle, WGM + 1 μM ddC, or WGM + 12 μM ddC. Treatment media were refreshed every 3 days. On days 6 and 13 post-treatment two of each of the 0, 1, and 12 μM ddC-treated cell culture dishes were separately harvested

(Fig. 3A). The medium was removed from each tissue culture dish to be harvested, and cells were gently washed with pre-warmed DPBS followed by trypsinization and neutralization with their respective treatment media. The proliferating cells were completely suspended in treatment media + trypsin by gently pipetting up and down until the mixture appeared homogenous. The cells were transferred to conical tubes and a small aliquot was removed for counting. The cells were centrifuged at 250g for 5 min, washed in DPBS (6 ml per  $1 \times 10^7$  cells), and then resuspended in 2 ml DPBS per  $1 \times 10^7$  cells. One milliliter of the resuspension was added to each of two 1.5-ml microcentrifuge tubes. The tubes were centrifuged at 250g for 5 min at 4 °C, the supernatant was aspirated, and the cell pellets were stored at -80 °C. The experiment was performed three times. Whole-cell DNA was extracted from cell pellets as described below under “Whole-cell DNA extraction from HepaRG cell pellets.”

### **ddC treatment of differentiated HepaRG for whole-cell DNA extraction**

Proliferating HepaRG cells were differentiated as described above under “HepaRG cell culture and differentiation.” The WDM treatment media were prepared by adding ddC to a final concentration of 0, 1, or 12  $\mu$ M. Cell culture dishes containing differentiated HepaRG were used to separately treat cells with 0, 1, or 12  $\mu$ M ddC by replacing the WDM with WDM + vehicle, WDM + 1  $\mu$ M ddC, or WDM + 12  $\mu$ M ddC, respectively. The treatment media were refreshed every 3 days. On days 6 and 13 post-treatment two of each of the 0, 1, and 12  $\mu$ M ddC-treated cell culture dishes were harvested (Fig. 3A). Treatment media were removed from each dish, and cells were washed with prewarmed DPBS followed by trypsinization and neutralization with their respective treatment media. The differentiated cells were completely suspended in the treatment media plus trypsin by gently pipetting up and down until the mixture appeared homogenous. Cells were counted, washed with DPBS, and frozen at -80 °C as described above for proliferating HepaRG. Whole-cell DNA was extracted from cell pellets as described below.

### **ddC treatment of proliferating HepaRG for seeding Seahorse XFp miniplates**

Proliferating HepaRG were seeded into tissue culture dishes and treated with ddC as described above under “ddC treatment of proliferating HepaRG for whole-cell DNA extraction.” On days 7 and 13 post treatment, two of each of the 0, 1, and 12  $\mu$ M ddC-treated cell culture dishes were separately harvested, Seahorse cell culture miniplate wells were seeded, and bioenergetics was evaluated the following day using the Seahorse XFp Extracellular Flux Analyzer (Fig. 3A). On days of harvesting the cells, the treatment media were removed; cells were gently washed with prewarmed DPBS, trypsinized, neutralized with treatment media, and counted as described above. The suspensions of ddC-treated proliferating HepaRG were diluted down in treatment media such that the Seahorse cell culture miniplate wells were seeded with  $1 \times 10^4$  cells per

well ( $9.4 \times 10^4$  cells/cm<sup>2</sup>) in the treatment media (WGM +0, 1, or 12  $\mu$ M ddC). The miniplates were incubated overnight at 37 °C, 5% CO<sub>2</sub> in a humidified incubator followed by Seahorse extracellular flux analysis. The leftover cells that were not used to seed Seahorse miniplate wells were washed with DPBS, pelleted, and stored at -80 °C.

### **ddC treatment of differentiated HepaRG for seeding Seahorse XFp miniplates**

Proliferating HepaRG cells were differentiated and treated with ddC as described above in “ddC treatment of differentiated HepaRG for whole-cell DNA extraction.” On days 7 and 13 post-treatment, two of each of the 0, 1, and 12  $\mu$ M ddC-treated cell culture dishes were harvested, cells were counted and then seeded into Seahorse cell culture miniplates as described above for proliferating HepaRG except that the WDM treatment media were used in place of WGM treatment media (Fig. 3A). Miniplates were incubated overnight at 37 °C, 5% CO<sub>2</sub> in a humidified incubator followed by Seahorse extracellular flux analysis. The leftover cells that were not used to seed Seahorse miniplate wells were washed with DPBS, pelleted, and stored at -80 °C.

### **Whole-cell DNA extraction from HepaRG cell pellets**

Whole-cell DNA extracts were prepared based on the protocol developed by Kolesar *et al.* (78). Briefly, HepaRG proliferating or differentiated cell pellets were thawed and digested overnight at 55 °C in 500  $\mu$ l proteinase K digestion buffer (100 mM Tris-Cl pH 8, 5 mM EDTA, 0.2% SDS, 200 mM NaCl, 0.3 mg/ml proteinase K, 1.1 mM 2-mercaptoethanol). The next morning, 10  $\mu$ l of proteinase K digestion buffer was added to each sample, gently mixed, and incubated for 1 h at 55 °C. Cellular protein was removed from the samples by adding NaCl to a final concentration of 1.25 M, pelleting at 15,000g for 15 min, and collecting the supernatant into a fresh microcentrifuge tube. The total nucleic acid was precipitated from the supernatant *via* ethanol precipitation. The pellets were dried away from light for ~1 h then resuspended in 1 $\times$  TE buffer (10 mM Tris-Cl, pH 8.0, 1 mM EDTA) plus 1 mM dimethyl urea. Samples were stored in the absence of light at room temperature overnight then frozen at -20 °C. The whole-cell DNA concentrations were measured in  $\geq$ triplicate using a Qubit fluorometer (Thermo Fisher Scientific) according to the manufacturer’s specifications.

### **Synthesis of digoxigenin-labeled probes, Southern blotting, and immunodetection of target DNA fragments**

Nuclear DNA (nDNA)- and mitochondrial DNA (mtDNA)-specific probes used for Southern blotting and immunodetection of target DNA fragments were synthesized *via* PCR using the PCR DIG Probe Synthesis Kit (Roche) as described (79). Briefly, each probe was synthesized separately from their respective plasmid templates. The pCR2.1-TOPO-18S plasmid harbors a cloned fragment of the human nuclear 18S ribosomal pseudogene 4 (RNA18SP4), and the pCR2.1-TOPO-mtDNA plasmid harbors a cloned fragment of the human

## Utilizing HepaRG to understand ddC mitochondrial toxicity

mtDNA sequence from nucleotide positions 168 to 604. Twenty-five-microliter PCR reactions for each probe contained 50 pg plasmid, 1× PCR buffer with 1.5 mM MgCl<sub>2</sub>, 0.5 μM of each respective primer, 1× PCR DIG Probe Synthesis mix, and 52.5 mU/μl of Expand High Fidelity Enzyme. 18S rDNA probe reactions contained 200 μM dATP, dCTP, and dGTP, as well as 130 μM dTTP and 70 μM DIG-11-dUTP. When synthesizing the mtDNA probe it is necessary to use a final DIG-11-dUTP concentration of 35 μM owing to the high GC content in pCR2.1-TOPO-mtDNA. In addition, the mtDNA probe reactions contained 200 μM dATP, dCTP, and dGTP, as well as 165 μM dTTP. PCR Thermocycling conditions were: initial denaturation for 2 min at 95 °C, 32 cycles of denaturing for 30 s at 95 °C, annealing for 30 s at 60 °C, and extension for 40 s at 72 °C. A final extension for 4 min at 72 °C was carried out. DIG-labeled probes were heated by boiling in a water bath for 5 min followed by rapid cooling on ice. Two microliters of heat-denatured mtDNA probe and 4 μl of 18S rDNA were added per milliliter of prehybridization solution (Roche) prewarmed to 50 °C for simultaneous detection of both probed sequences in BamHI-digested whole-cell DNA extracts. The probe mixture was used immediately or stored at -20 °C until needed.

One microgram of whole-cell extracted DNA was digested with 5 units of BamHI (Thermo Scientific) in a 1× digestion buffer for 3 h at 37 °C. The digested samples were loaded on to 1.0% agarose gels in 1× TAE buffer (40 mM Tris, 20 mM acetic acid, 1 mM EDTA) without ethidium bromide and were electrophoresed at 20 V for 16 h. Gels were soaked in 0.25 N HCl for 5 min to partially depurinate the DNA. Next, gels were rinsed in sterile Milli-Q water, soaked twice in denaturing solution (0.5 N NaOH, 1.5 M NaCl) for 15 min, rinsed in autoclaved Milli-Q water, and then soaked twice in neutralizing solution (0.5 M Tris-HCl, pH 7.5, 3 M NaCl) for 15 min. These steps allow for in-gel DNA denaturation and fragmentation of high-molecular-weight DNA molecules (e.g., the 16.6-kb mtDNA) into smaller pieces to allow efficient transfer to the membrane during Southern blotting. An electrophoresis gel tray was placed upside down inside a container filled halfway up the gel tray with 20× SSC buffer (3 M NaCl, 0.3 M sodium citrate, pH 7.0). A long piece of 20× SSC-soaked Whatman paper was placed on top of the gel tray with ends angled down into the 20× SSC buffer to act as a wick. The gel was rinsed once more in water then placed on top of the wick. A piece of Amersham Hybond - N<sup>+</sup> positively charged membrane (GE Healthcare Life Sciences) cut slightly larger than the gel was soaked in 2× SSC buffer for 1 min then placed on top of the gel. Two pieces of Whatman paper cut the same size as the membrane were soaked in 2× SSC then placed on top of the membrane and a test tube was used to roll out any bubbles. An ~5-cm stack of paper towels cut slightly smaller than membrane was placed on top of Whatman papers and a 200-g weight was used to allow the capillary transfer of DNA to the membrane overnight. The Southern blot was disassembled and all paper towels were discarded. The membrane

was placed onto a Fotodyne transilluminator and exposed to UV light for 2 min to cross-link DNA onto it. The membrane was rinsed in water and allowed to air dry.

Southern blot membranes were placed into 35 × 150-mm hybridization bottles with 6 ml of prehybridization solution (Roche) and incubated in a hybridization oven for 2 to 3 h at 50 °C. The prehybridization solution was discarded and replaced with the dual probe solution then incubated at 50 °C overnight. On the next day, probe solutions were removed and membranes were washed twice in 2× SSC + 0.1% SDS for 5 min at room temperature in the hybridization oven. Next, the blots were washed twice with prewarmed 0.5× SSC + 0.1% SDS at 65 °C for 15 min. The membranes were removed from hybridization bottles and equilibrated in a maleic acid buffer (0.1 M maleic acid, 0.15 M NaCl, pH 7.5) for 2 min by mixing on an orbital shaker at 50 rpm then placed in 40 ml 1× blocking buffer (Roche) + 0.015% SDS and mixed for 30 min. The blocking buffer was made by adding 100 ml of 10× blocking buffer (Roche) to 900 ml of maleic acid buffer. The anti-DIG alkaline phosphatase conjugate (Roche) was added to the blocking solution + 0.015% SDS at 75 mU/ml and membranes were incubated for ~1 h with mixing. The blocking solution containing the antibody was discarded, the membrane was rinsed three times with Milli-Q water, then the membrane was washed twice with wash buffer (maleic acid buffer, 0.3% Tween20, 0.015% SDS) by mixing for 15 min. The wash buffer was discarded and replaced with the detection buffer (0.1 M Tris-HCl, 0.1 M NaCl, pH 9.5) for 3 min. The CDP-star solution was made by mixing 10 μl of 25 mM CDP-Star (Roche) with 0.99 ml of detection buffer in a microcentrifuge tube. The membrane was removed from the detection buffer and placed on clear plastic wrap. The CDP-star substrate was evenly distributed onto the membrane and incubated for 1 min at room temperature. The membrane was then placed on another piece of plastic wrap, and the plastic wrap was folded over the membrane to keep it wet. The membrane was incubated at 37 °C for 5 min then imaged using Syngene G:Box.

### Estimation of mtDNA copy number utilizing a pCR2.1-TOPO-mtDNA standard curve

Cell counts, DNA concentrations, and Southern blot data were utilized to estimate the mtDNA copy number. Standard curves were generated using a series of dilutions of the pCR2.1-TOPO-mtDNA plasmid, the same plasmid that was used to synthesize the DIG-labeled mtDNA probe. The pCR2.1-TOPO-mtDNA plasmid harbors a cloned fragment of the human HEK-293 (ATCC CRL-1573) mtDNA sequence from nucleotide positions 168 to 604, and this sequence differs from the NC\_012920.1 reference sequence at three positions: 263 A>G, 309\_310insC, and 315\_316insC. Digestion with HindIII that cuts the plasmid once upstream of the mtDNA sequence in the polylinker linearized pCR2.1-TOPO-mtDNA. The plasmid was isolated using the Omega Bio-Tek E.Z.N.A. Plasmid DNA Mini Kit II. The plasmid DNA was digested with 5 U/μg of HindIII for 3 h at 37 °C. Next, the linearized plasmid

was run on an agarose gel for 1 h at 100 V, the plasmid bands were cut out of the gel, and the gel was extracted using the Omega Bio-Tek E.Z.N.A. Gel Extraction Kit. The gel extracted plasmid DNA concentration was measured in triplicate using a Qubit fluorometer. The plasmid was diluted down to 0.696 ng/ $\mu$ l, then the plasmid concentration was measured again in triplicate. Ten microliters of 0.696 ng/ $\mu$ l plasmid was loaded onto gels along with 10  $\mu$ l of two 2-fold serially diluted samples, 0.348 and 0.174 ng/ $\mu$ l. We assume that the probe will hybridize to the plasmid and the mtDNA sequences identically. One microgram of WCE DNA samples was loaded along with the plasmid samples, and linear regression analysis was utilized to estimate the copies of differentiated HepaRG mtDNA in each 1  $\mu$ g WCE DNA sample. As the 4.4-kb plasmid and the 16.6-kb mtDNA differ in size by 12.2-kb, 1 ng of plasmid contains the same number of molecules as 3.8 ng of mtDNA.

### Seahorse XFp bioenergetic analysis

The Seahorse XFp extracellular flux analyzer was used to measure bioenergetics as previously described (31). Briefly,  $1 \times 10^4$  proliferating or differentiated HepaRG cells were treated sequentially with 2  $\mu$ M oligomycin, 1  $\mu$ M carbonyl cyanide p-trifluoromethoxy-phenylhydrazone (FCCP), and 0.5  $\mu$ M antimycin A + 0.5  $\mu$ M rotenone (all purchased from Fisher Scientific). After the experiments, cells were gently washed with 200  $\mu$ l prewarmed DPBS, incubated overnight at  $-80^\circ\text{C}$ , then lysed in ice-cold RIPA lysis buffer (50 mM Tris-Cl pH 8.0, 150 mM NaCl, 1% Igepal CA-630, 0.5% deoxycholate, 0.1% sodium dodecyl sulfate) supplemented with a 1 in 101 dilution of HALT protease inhibitor cocktail (Thermo Fisher Scientific). The total cellular protein content in each miniplate well was measured using the Pierce bicinchoninic acid protein assay kit (Thermo Scientific), and OCR and ECAR values were normalized to total cellular protein. Data were obtained from three independent experiments performed on different days and are presented as mean  $\pm$  standard deviation (SD).

### Equations used to calculate mitochondrial respiration parameters

Mitochondrial respiration parameters were calculated as follows: *I. Basal respiration* = (Last rate before the first injection) – (Nonmitochondrial respiration rate), *II. Proton leak* = (Minimum rate after oligomycin injection) – (Nonmitochondrial respiration rate), *III. Maximal respiratory capacity* = (Maximum rate after FCCP injection) – (Nonmitochondrial respiration rate), *IV. Spare respiratory capacity or reserve respiratory capacity* = (Maximal respiratory capacity) – (Basal respiration), *V. Nonmitochondrial respiration* = Minimum rate after rotenone + antimycin A injection, *VI. ATP-linked respiration* = (Last rate before oligomycin injection) – (Minimum rate after oligomycin injection) (53).

### Statistical analyses used

For the analysis of bioenergetics data, statistical analysis was run using a three-way ANOVA (*i.e.*,  $2 \times 2 \times 3$ ) with follow-up

post hoc tests to determine significance. We examined the cell type (proliferating or differentiated), day (8 or 14), and concentration (0, 1, and 12  $\mu$ M ddC) for each variable of interest. SAS software version 9.4 was used for data analysis. For analyses of all other data, statistical significance between two parametric groups with unequal variance was determined using a Welch's *t* test. Comparisons of more than two groups of parametric data were assessed by one-way analysis of variance (ANOVA) followed by Tukey's test or Welch's ANOVA with Games–Howell post hoc. Comparisons of greater than two groups of nonparametric data were assessed by Kruskal–Wallis tests followed by Dunn's post hoc test. *p*-values less than 0.05 were considered significant.

### Data availability

All of the data described herein is within this article. Reagents, plasmids, etc., are available upon request by contacting the corresponding author M. J. Y.

**Acknowledgments**—We thank Dr Kristin Delfino for assistance with statistical analyses of data and Drs Deborah A. Court and Chris Weston for critically reading this manuscript. We gratefully acknowledge the work of Drs Christiane Guguen-Guillouzo, Philippe Gripon, and Christian Trepo for the isolation and characterization of HepaRG. Also, the technical assistance of Grace Forrest is acknowledged. We thank the anonymous reviewers whose comments and suggestions improved and clarified the content of this work.

**Author contributions**—M. J. Y. Conceptualization; M. J. Y., C. K. J. Y., and J. H. W. Methodology; M. J. Y., C. K. J. Y., and J. H. W. Formal Analysis; M. J. Y., C. K. J. Y., J. H. W., and M. M. R. Investigation; M. J. Y. Resources; M. J. Y., C. K. J. Y., J. H. W., and M. M. R. Data Curation; M. J. Y. Writing – Original Draft Preparation; M. J. Y., and C. K. J. Y. Writing – Review & Editing; M.J.Y. Supervision; M.J.Y. Project Administration; M. J. Y. Funding Acquisition.

**Funding and additional information**—This research was supported by a National Institute of Environmental Health Sciences Pathway to Independence Award to M. J. Y. (5R00ES022638-04), by start-up funds from SIU School of Medicine to M.J.Y., and by an SIU Carbondale Doctoral Research Fellowship to M. M. R.

**Conflict of interest**—The authors declare that they have no conflicts of interest with the contents of this article.

**Abbreviations**—The abbreviations used are: 3TC, 2',3'-dideoxy-3'-thiacytidine; ANT, adenine nucleotide translocase; APAP or paracetamol, acetaminophen; AZT, 3' -azido-2',3' -dideoxythymidine; CBV, carbocyclic 2',3'-didehydro-2',3'-dideoxyguanosine; CO<sub>2</sub>, carbon dioxide; ddC, zalcitabine, 2'-3'-dideoxycytidine; ddCMP, 2'-3'-dideoxycytidine 5'-monophosphate; ddCTP, 2'-3'-dideoxycytidine 5'-triphosphate; ddi, 2',3'-dideoxyinosine; DIG-11-dUTP, digoxigenin-11-deoxy-uridine-triphosphate, alkali-labile; DPBS, Dulbecco's phosphate-buffered saline; ECAR, extracellular acidification rate; FCCP, carbonyl cyanide p-trifluoromethoxy-phenylhydrazone; H<sub>2</sub>O, water; MIM, mitochondrial inner membrane; mtDNA, mitochondrial DNA; nDNA, nuclear DNA; NRTI, nucleoside reverse-transcriptase inhibitor; NtRTIs, nucleotide reverse

## Utilizing HepaRG to understand ddC mitochondrial toxicity

transcriptase inhibitors; OCR, oxygen consumption rate; OXPHOS, oxidative phosphorylation; PBL, peripheral blood lymphocyte; Poly, mtDNA polymerase gamma; RPTEC, renal proximal tubule epithelial cell; SkMC, skeletal muscle cell; WCE, whole-cell extracted; WDM, Working Differentiation Medium; WGM, Working Growth Medium.

### References

1. Eggleton, J. S., and Nagalli, S. (2020) *Highly Active Antiretroviral Therapy (HAART)*, StatPearls, Treasure Island (FL)
2. Berger, A. R., Arezzo, J. C., Schaumburg, H. H., Skowron, G., Merigan, T., Bozzette, S., Richman, D., and Soo, W. (1993) 2',3'-dideoxycytidine (ddC) toxic neuropathy: a study of 52 patients. *Neurology* **43**, 358–362
3. Young, M. J. (2017) Off-target effects of drugs that disrupt human mitochondrial DNA maintenance. *Front. Mol. Biosci.* **4**, 74
4. Lewis, W., Copeland, W. C., and Day, B. (2001) Mitochondrial DNA depletion, oxidative stress and mutation: mechanisms of nucleoside reverse transcriptase inhibitor toxicity. *Lab. Invest.* **81**, 777–790
5. Zhu, C., Johansson, M., and Karlsson, A. (2000) Incorporation of nucleoside analogs into nuclear or mitochondrial DNA is determined by the intracellular phosphorylation site. *J. Biol. Chem.* **275**, 26727–26731
6. Liyanage, S. U., Hurren, R., Voisin, V., Bridon, G., Wang, X., Xu, C., MacLean, N., Siriwardena, T. P., Gronda, M., Yehudai, D., Sriskanthadevan, S., Avizonis, D., Shamas-Din, A., Minden, M. D., Bader, G. D., et al. (2017) Leveraging increased cytoplasmic nucleoside kinase activity to target mtDNA and oxidative phosphorylation in AML. *Blood* **129**, 2657–2666
7. Lim, S. E., and Copeland, W. C. (2001) Differential incorporation and removal of antiviral deoxynucleotides by human DNA polymerase gamma. *J. Biol. Chem.* **276**, 23616–23623
8. Hanes, J. W., and Johnson, K. A. (2008) Exonuclease removal of dideoxycytidine (zalcitabine) by the human mitochondrial DNA polymerase. *Antimicrob. Agents Chemother.* **52**, 253–258
9. Johnson, A. A., Ray, A. S., Hanes, J., Suo, Z., Colacino, J. M., Anderson, K. S., and Johnson, K. A. (2001) Toxicity of antiviral nucleoside analogs and the human mitochondrial DNA polymerase. *J. Biol. Chem.* **276**, 40847–40857
10. Brown, J. A., Pack, L. R., Fowler, J. D., and Suo, Z. (2012) Presteady state kinetic investigation of the incorporation of anti-hepatitis B nucleotide analogues catalyzed by noncanonical human DNA polymerases. *Chem. Res. Toxicol.* **25**, 225–233
11. Birkus, G., Hitchcock, M. J., and Cihlar, T. (2002) Assessment of mitochondrial toxicity in human cells treated with tenofovir: comparison with other nucleoside reverse transcriptase inhibitors. *Antimicrob. Agents Chemother.* **46**, 716–723
12. Setzer, B., Schlesier, M., Thomas, A. K., and Walker, U. A. (2005) Mitochondrial toxicity of nucleoside analogues in primary human lymphocytes. *Antivir. Ther.* **10**, 327–334
13. Feng, J. Y., Xu, Y., Barauskas, O., Perry, J. K., Ahmadyar, S., Stepan, G., Yu, H., Babusis, D., Park, Y., McCutcheon, K., Perron, M., Schultz, B. E., Sakowicz, R., and Ray, A. S. (2016) Role of mitochondrial RNA polymerase in the toxicity of nucleotide inhibitors of hepatitis C virus. *Antimicrob. Agents Chemother.* **60**, 806–817
14. Martin, J. L., Brown, C. E., Matthews-Davis, N., and Reardon, J. E. (1994) Effects of antiviral nucleoside analogs on human DNA polymerases and mitochondrial DNA synthesis. *Antimicrob. Agents Chemother.* **38**, 2743–2749
15. Medina, D. J., Tsai, C. H., Hsiung, G. D., and Cheng, Y. C. (1994) Comparison of mitochondrial morphology, mitochondrial DNA content, and cell viability in cultured cells treated with three anti-human immunodeficiency virus dideoxynucleosides. *Antimicrob. Agents Chemother.* **38**, 1824–1828
16. Jemt, E., Persson, O., Shi, Y., Mehmedovic, M., Uhler, J. P., Davila Lopez, M., Freyer, C., Gustafsson, C. M., Samuelsson, T., and Falkenberg, M. (2015) Regulation of DNA replication at the end of the mitochondrial D-loop involves the helicase TWINKLE and a conserved sequence element. *Nucleic Acids Res.* **43**, 9262–9275
17. Fernández-Moreno, M., Hermida-Gómez, T., Gallardo, M. E., Dalmao-Fernández, A., Rego-Pérez, I., Garesse, R., and Blanco, F. J. (2016) Generating Rho-0 cells using mesenchymal stem cell lines. *PLoS One* **11**, e0164199
18. Will, Y., Shields, J. E., and Wallace, K. B. (2019) Drug-induced mitochondrial toxicity in the geriatric population: challenges and future directions. *Biology (Basel)* **8**, 32
19. Meyer, J. N., Hartman, J. H., and Mello, D. F. (2018) Mitochondrial toxicity. *Toxicol. Sci.* **162**, 15–23
20. Meyer, J. N., Leung, M. C., Rooney, J. P., Sendoel, A., Hengartner, M. O., Kisby, G. E., and Bess, A. S. (2013) Mitochondria as a target of environmental toxicants. *Toxicol. Sci.* **134**, 1–17
21. Nadanaciva, S., Rana, P., Beeson, G. C., Chen, D., Ferrick, D. A., Beeson, C. C., and Will, Y. (2012) Assessment of drug-induced mitochondrial dysfunction via altered cellular respiration and acidification measured in a 96-well platform. *J. Bioenerg. Biomembr.* **44**, 421–437
22. Attene-Ramos, M. S., Huang, R., Sakamuru, S., Witt, K. L., Beeson, G. C., Shou, L., Schnellmann, R. G., Beeson, C. C., Tice, R. R., Austin, C. P., and Xia, M. (2013) Systematic study of mitochondrial toxicity of environmental chemicals using quantitative high throughput screening. *Chem. Res. Toxicol.* **26**, 1323–1332
23. Soldatow, V. Y., Lecluyse, E. L., Griffith, L. G., and Rusyn, I. (2013) Models for liver toxicity testing. *Toxicol. Res. (Camb.)* **2**, 23–39
24. Huang, R., Xia, M., Sakamuru, S., Zhao, J., Shahane, S. A., Attene-Ramos, M., Zhao, T., Austin, C. P., and Simeonov, A. (2016) Modelling the Tox21 10 K chemical profiles for *in vivo* toxicity prediction and mechanism characterization. *Nat. Commun.* **7**, 10425
25. Gripon, P., Rumin, S., Urban, S., Le Seyec, J., Glaise, D., Cannie, I., Guyomard, C., Lucas, J., Trepo, C., and Guguen-Guillouzo, C. (2002) Infection of a human hepatoma cell line by hepatitis B virus. *Proc. Natl. Acad. Sci. U. S. A.* **99**, 15655–15660
26. Tascher, G., Burban, A., Camus, S., Plumel, M., Chanon, S., Le Guevel, R., Shevchenko, V., Van Dorsselaer, A., Lefai, E., Guguen-Guillouzo, C., and Bertile, F. (2019) In-depth proteome analysis highlights HepaRG cells as a versatile cell system surrogate for primary human hepatocytes. *Cells* **8**, 192
27. Anthérieu, S., Chesné, C., Li, R., Camus, S., Lahoz, A., Picazo, L., Turpeinen, M., Tolonen, A., Uusitalo, J., Guguen-Guillouzo, C., and Guillouzo, A. (2010) Stable expression, activity, and inducibility of cytochromes P450 in differentiated HepaRG cells. *Drug Metab. Dispos.* **38**, 516–525
28. Aninat, C., Piton, A., Glaise, D., Le Charpentier, T., Langouët, S., Morel, F., Guguen-Guillouzo, C., and Guillouzo, A. (2006) Expression of cytochromes P450, conjugating enzymes and nuclear receptors in human hepatoma HepaRG cells. *Drug Metab. Dispos.* **34**, 75–83
29. van Wenum, M., Adam, A. A., Hakvoort, T. B., Hendriks, E. J., Shevchenko, V., van Gulik, T. M., Chamuleau, R. A., and Hoekstra, R. (2016) Selecting cells for bioartificial liver devices and the importance of a 3D culture environment: a functional comparison between the HepaRG and C3A cell lines. *Int. J. Biol. Sci.* **12**, 964–978
30. Marion, M. J., Hantz, O., and Durantal, D. (2010) The HepaRG cell line: biological properties and relevance as a tool for cell biology, drug metabolism, and virology studies. *Methods Mol. Biol.* **640**, 261–272
31. Young, C. K. J., and Young, M. J. (2019) Comparison of HepaRG cells following growth in proliferative and differentiated culture conditions reveals distinct bioenergetic profiles. *Cell Cycle* **18**, 476–499
32. Young, M. J., Jayaprakash, A. D., and Young, C. K. J. (2019) Analysis of mitochondrial DNA polymorphisms in the human cell lines HepaRG and SJCRH30. *Int. J. Mol. Sci.* **20**, 3245
33. Seley-Radtke, K. L., and Yates, M. K. (2018) The evolution of nucleoside analogue antivirals: a review for chemists and non-chemists. Part I: early structural modifications to the nucleoside scaffold. *Antiviral Res.* **154**, 66–86
34. De Clercq, E., Balzarini, J., Descamps, J., and Eckstein, F. (1980) Antiviral, antimetabolic and antineoplastic activities of 2'- or 3'-amino or -azido-substituted deoxyribonucleosides. *Biochem. Pharmacol.* **29**, 1849–1851
35. Feng, J. Y. (2018) Addressing the selectivity and toxicity of antiviral nucleosides. *Antivir. Chem. Chemother.* **26**, 2040206618758524

36. Elwell, L. P., Ferone, R., Freeman, G. A., Fyfe, J. A., Hill, J. A., Ray, P. H., Richards, C. A., Singer, S. C., Knick, V. B., Rideout, J. L., and Zimmerman, T. P. (1987) Antibacterial activity and mechanism of action of 3'-azido-3'-deoxythymidine (BW A509U). *Antimicrob. Agents Chemother.* **31**, 274–280
37. De Clercq, E. (2011) A 40-year journey in search of selective antiviral chemotherapy. *Annu. Rev. Pharmacol. Toxicol.* **51**, 1–24
38. Wallace, D. C. (2012) Mitochondria and cancer. *Nat. Rev. Cancer.* **12**, 685–698
39. Louat, T., Servant, L., Rols, M. P., Bieth, A., Teissie, J., Hoffmann, J. S., and Cazaux, C. (2001) Antitumor activity of 2',3'-dideoxycytidine nucleotide analog against tumors up-regulating DNA polymerase beta. *Mol. Pharmacol.* **60**, 553–558
40. Aschacher, T., Sampl, S., Kaser, L., Bernhard, D., Spittler, A., Holzmann, K., and Bergmann, M. (2012) The combined use of known antiviral reverse transcriptase inhibitors AZT and DDI induce anticancer effects at low concentrations. *Neoplasia* **14**, 44–53
41. Bogenhagen, D., and Clayton, D. A. (1977) Mouse L cell mitochondrial DNA molecules are selected randomly for replication throughout the cell cycle. *Cell* **11**, 719–727
42. Pontarin, G., Fijolek, A., Pizzo, P., Ferraro, P., Rampazzo, C., Pozzan, T., Thelander, L., Reichard, P. A., and Bianchi, V. (2008) Ribonucleotide reduction is a cytosolic process in mammalian cells independently of DNA damage. *Proc. Natl. Acad. Sci. U. S. A.* **105**, 17801–17806
43. Saada, A., Shaag, A., and Elpeleg, O. (2003) mtDNA depletion myopathy: elucidation of the tissue specificity in the mitochondrial thymidine kinase (TK2) deficiency. *Mol. Genet. Metab.* **79**, 1–5
44. Papa, S. (1996) Mitochondrial oxidative phosphorylation changes in the life span. Molecular aspects and physiopathological implications. *Biochim. Biophys. Acta* **1276**, 87–105
45. Saada, A., Shaag, A., Mandel, H., Nevo, Y., Eriksson, S., and Elpeleg, O. (2001) Mutant mitochondrial thymidine kinase in mitochondrial DNA depletion myopathy. *Nat. Genet.* **29**, 342–344
46. Tang, Y., Schon, E. A., Wilichowski, E., Vazquez-Memije, M. E., Davidson, E., and King, M. P. (2000) Rearrangements of human mitochondrial DNA (mtDNA): new insights into the regulation of mtDNA copy number and gene expression. *Mol. Biol. Cell* **11**, 1471–1485
47. Benbrik, E., Charriot, P., Bonavaud, S., Ammi-Said, M., Frisdal, E., Rey, C., Gherardi, R., and Barlovatz-Meimon, G. (1997) Cellular and mitochondrial toxicity of zidovudine (AZT), didanosine (ddI) and zalcitabine (ddC) on cultured human muscle cells. *J. Neurol. Sci.* **149**, 19–25
48. Klecker, R. W., Jr., Collins, J. M., Yarchoan, R. C., Thomas, R., McAtee, N., Broder, S., and Myers, C. E. (1988) Pharmacokinetics of 2',3'-dideoxycytidine in patients with AIDS and related disorders. *J. Clin. Pharmacol.* **28**, 837–842
49. Borg, N., and Stahle, L. (1998) Pharmacokinetics and distribution over the blood-brain barrier of zalcitabine (2',3'-dideoxycytidine) and BEA005 (2',3'-dideoxy-3'-hydroxymethylcytidine) in rats, studied by microdialysis. *Antimicrob. Agents Chemother.* **42**, 2174–2177
50. Nadanaciva, S., Dillman, K., Gebhard, D. F., Shrikhande, A., and Will, Y. (2010) High-content screening for compounds that affect mtDNA-encoded protein levels in eukaryotic cells. *J. Biomol. Screen* **15**, 937–948
51. Rocher, C., Taanman, J. W., Pierron, D., Faustin, B., Benard, G., Rossignol, R., Malgat, M., Pedespan, L., and Letellier, T. (2008) Influence of mitochondrial DNA level on cellular energy metabolism: implications for mitochondrial diseases. *J. Bioenerg. Biomembr.* **40**, 59–67
52. Ashley, N., Harris, D., and Poulton, J. (2005) Detection of mitochondrial DNA depletion in living human cells using PicoGreen staining. *Exp. Cell Res.* **303**, 432–446
53. Divakaruni, A. S., Paradise, A., Ferrick, D. A., Murphy, A. N., and Jastroch, M. (2014) Analysis and interpretation of microplate-based oxygen consumption and pH data. *Methods Enzymol.* **547**, 309–354
54. van der Windt, G. J., Everts, B., Chang, C. H., Curtis, J. D., Freitas, T. C., Amiel, E., Pearce, E. J., and Pearce, E. L. (2012) Mitochondrial respiratory capacity is a critical regulator of CD8+ T cell memory development. *Immunity* **36**, 68–78
55. Brand, M. D. (2005) The efficiency and plasticity of mitochondrial energy transduction. *Biochem. Soc. Trans.* **33**, 897–904
56. Peeva, V., Blei, D., Trombly, G., Corsi, S., Szukszto, M. J., Rebelo-Guioimar, P., Gammage, P. A., Kudin, A. P., Becker, C., Altmuller, J., Minczuk, M., Zsurka, G., and Kunz, W. S. (2018) Linear mitochondrial DNA is rapidly degraded by components of the replication machinery. *Nat. Commun.* **9**, 1727
57. Young, M. J., and Copeland, W. C. (2016) Human mitochondrial DNA replication machinery and disease. *Curr. Opin. Genet. Dev.* **38**, 52–62
58. Stephan, T., Roesch, A., Riedel, D., and Jakobs, S. (2019) Live-cell STED nanoscopy of mitochondrial cristae. *Sci. Rep.* **9**, 12419
59. Bogenhagen, D. F., Rousseau, D., and Burke, S. (2008) The layered structure of human mitochondrial DNA nucleoids. *J. Biol. Chem.* **283**, 3665–3675
60. Feng, J. Y., Cheng, G., Perry, J., Barauskas, O., Xu, Y., Fenaux, M., Eng, S., Tirunagari, N., Peng, B., Yu, M., Tian, Y., Lee, Y. J., Stepan, G., Laggapan, L. L., Jin, D., et al. (2014) Inhibition of hepatitis C virus replication by GS-6620, a potent C-nucleoside monophosphate prodrug. *Antimicrob. Agents Chemother.* **58**, 1930–1942
61. Le Guillou, D., Bucher, S., Begriche, K., Hoet, D., Lombes, A., Labbe, G., and Fromenty, B. (2018) Drug-induced alterations of mitochondrial DNA homeostasis in steatotic and nonsteatotic HepaRG cells. *J. Pharmacol. Exp. Ther.* **365**, 711–726
62. Kholodenko, I. V., and Yarygin, K. N. (2017) Cellular mechanisms of liver regeneration and cell-based therapies of liver diseases. *Biomed. Res. Int.* **2017**, 8910821
63. Le Vee, M., Noel, G., Jouan, E., Stieger, B., and Fardel, O. (2013) Polarized expression of drug transporters in differentiated human hepatoma HepaRG cells. *Toxicol. In Vitro* **27**, 1979–1986
64. Antonelli, G., Turriziani, O., Cianfriglia, M., Riva, E., Dong, G., Fattorossi, A., and Dianzani, F. (1992) Resistance of HIV-1 to AZT might also involve the cellular expression of multidrug resistance P-glycoprotein. *AIDS Res. Hum. Retroviruses* **8**, 1839–1844
65. Schuetz, J. D., Connelly, M. C., Sun, D., Paibir, S. G., Flynn, P. M., Srinivas, R. V., Kumar, A., and Fridland, A. (1999) MRP4: a previously unidentified factor in resistance to nucleoside-based antiviral drugs. *Nat. Med.* **5**, 1048–1051
66. Ray, A. S., Cihlar, T., Robinson, K. L., Tong, L., Vela, J. E., Fuller, M. D., Wieman, L. M., Eisenberg, E. J., and Rhodes, G. R. (2006) Mechanism of active renal tubular efflux of tenofovir. *Antimicrob. Agents Chemother.* **50**, 3297–3304
67. Bratic, A., Kauppila, T. E., Macao, B., Gronke, S., Siibak, T., Stewart, J. B., Baggio, F., Dols, J., Partridge, L., Falkenberg, M., Wredenberg, A., and Larsson, N. G. (2015) Complementation between polymerase- and exonuclease-deficient mitochondrial DNA polymerase mutants in genomically engineered flies. *Nat. Commun.* **6**, 8808
68. Meyer, J. N., and Chan, S. S. L. (2017) Sources, mechanisms, and consequences of chemical-induced mitochondrial toxicity. *Toxicology* **391**, 2–4
69. Zolkipli-Cunningham, Z., and Falk, M. J. (2017) Clinical effects of chemical exposures on mitochondrial function. *Toxicology* **391**, 90–99
70. Roubicek, D. A., and Souza-Pinto, N. C. (2017) Mitochondria and mitochondrial DNA as relevant targets for environmental contaminants. *Toxicology* **391**, 100–108
71. Arnold, J. J., Sharma, S. D., Feng, J. Y., Ray, A. S., Smidansky, E. D., Kireeva, M. L., Cho, A., Perry, J., Vela, J. E., Park, Y., Xu, Y., Tian, Y., Babusis, D., Barauskas, O., Peterson, B. R., et al. (2012) Sensitivity of mitochondrial transcription and resistance of RNA polymerase II dependent nuclear transcription to antiviral ribonucleosides. *PLoS Pathog.* **8**, e1003030
72. Yamanaka, H., Gatanaga, H., Kosalaraksa, P., Matsuoka-Aizawa, S., Takahashi, T., Kimura, S., and Oka, S. (2007) Novel mutation of human DNA polymerase gamma associated with mitochondrial toxicity induced by anti-HIV treatment. *J. Infect. Dis.* **195**, 1419–1425
73. Bailey, C. M., Kasiviswanathan, R., Copeland, W. C., and Anderson, K. S. (2009) R964C mutation of DNA polymerase gamma imparts increased stavudine toxicity by decreasing nucleoside analog discrimination and impairing polymerase activity. *Antimicrob. Agents Chemother.* **53**, 2610–2612
74. Li, M., Mislak, A. C., Foli, Y., Agbosu, E., Bose, V., Bhandari, S., Szymanski, M. R., Shumate, C. K., Yin, Y. W., Anderson, K. S., and Paintsil, E. (2016) The DNA polymerase gamma R953C mutant is associated with

## Utilizing HepaRG to understand ddC mitochondrial toxicity

- antiretroviral therapy-induced mitochondrial toxicity. *Antimicrob. Agents Chemother.* **60**, 5608–5611
75. Chiappini, F., Teicher, E., Saffroy, R., Debuire, B., Vittecoq, D., and Lemoine, A. (2009) Relationship between polymerase gamma (POLG) polymorphisms and antiretroviral therapy-induced lipodystrophy in HIV-1 infected patients: a case-control study. *Curr. HIV Res.* **7**, 244–253
  76. Duong, V. N., Zhou, L., Martinez-Jimenez, M. I., He, L., Cosme, M., Blanco, L., Painsil, E., and Anderson, K. S. (2020) Identifying the role of PrimPol in TDF-induced toxicity and implications of its loss of function mutation in an HIV+ patient. *Sci. Rep.* **10**, 9343
  77. Saneto, R. P., and Naviaux, R. K. (2010) Polymerase gamma disease through the ages. *Dev. Disabil. Res. Rev.* **16**, 163–174
  78. Kolesar, J. E., Wang, C. Y., Taguchi, Y. V., Chou, S. H., and Kaufman, B. A. (2013) Two-dimensional intact mitochondrial DNA agarose electrophoresis reveals the structural complexity of the mammalian mitochondrial genome. *Nucleic Acids Res.* **41**, e58
  79. Wheeler, J. H., Young, C. K. J., and Young, M. J. (2019) Analysis of human mitochondrial DNA content by southern blotting and nonradioactive probe hybridization. *Curr. Protoc. Toxicol.* **80**, e75